A Szilikátipari Tudományos Egyesület lapja

építőanyag

Journal of Silicate Based and Composite Materials

A TARTALOMBÓL:

2023/2

We are pleased to welcome you to the 38th Şişecam International Glass Conference featuring the theme "Collaborate to Innovate: For a Sustainable Future." The event will be held in a hybrid format in Istanbul, Türkiye on November 2-3, 2023.

We believe that the 38th Şişecam International Glass Conference is an ideal opportunity to reach out to the world's leading scientists and researchers and discuss the constantly expanding usage areas and endless potential of glass in creating a sustainable future. By participating, you can inspire the glass community and help develop issues to be explored further.

Şişecam was founded to meet Türkiye's need for basic glass products. One of the most powerful industrial conglomerates in the country today, Şişecam has also transformed into a global player in all key areas of the glass industry, as well as in the soda and chromium compounds business lines. Aligned with its long-term vision, Şişecam commenced its corporate R&D activities in 1976 by establishing the first R&D center for glass science and technology in Türkiye. As a global player in the glass and chemicals industries, Şişecam continues to innovate and collaborate for a sustainable future.

Aligned with its long-term commitment to glass technology, Şişecam has conducted corporate R&D activities since 1976. Şişecam is the first company to establish an R&D center for glass science and technology in Türkiye.

Committed to better serving the global glass industry, Şişecam launched the Şişecam Glass Symposium in 1985. Over the following 37 years, the Symposium has steadily grown and evolved into an international event that now attracts hundreds of distinguished participants from industry and academia from around the world.

As one of Europe's premier glass science and technology platforms, the Şişecam Glass Symposium has been organized simultaneously with the International Commission on Glass (ICG) three times in the past. In 2019, Şişecam International Glass Conference and the 34th Şişecam Glass Symposium welcomed 500 participants from 26 countries in Istanbul. In 2020 and 2021, the symposiums were held online due to the Covid-19 pandemic. Last year, the 37th Şişecam International Glass Conference was held in a hybrid format; some 705 participants from 39 countries spanning five continents attended this event physically and virtually.

We are pleased to welcome you to the 38th Şişecam International Glass Conference featuring the theme "Collaborate to Innovate: For a Sustainable Future." The event will be held in a hybrid format in Istanbul, Türkiye on November 2-3, 2023.

We believe that the 38th Şişecam International Glass Conference is an ideal opportunity to reach out to the world's leading scientists and researchers and discuss the constantly expanding usage areas and endless potential of glass in creating a sustainable future. By participating, you can inspire the glass community and help develop issues to be explored further.

glassconference.sisecam.com

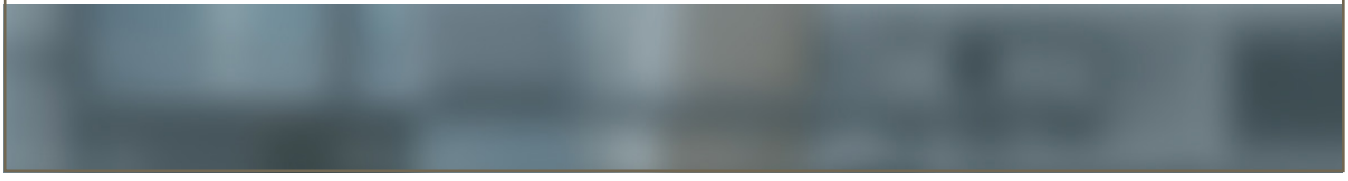

építőanyag

Journal of Silicate Based and Composite Materials

2023/2

TARTALOM

CONTENT

A finomkerámia-, üveg-, cement-, mész-, beton-, tégla- és cserép-, kő- és kavics-, tűzállóanyag-, szigetelőanyag-iparágak szakmai lapja
Scientific journal of ceramics, glass, cement, concrete, clay products, stone and gravel, insulating and fireproof materials and composites

A folyóiratot referálja · The journal is referred by:

A folyóiratban lektorált cikkek jelennek meg.
All published papers are peer-reviewed.
Kiadó · Publisher: Szilikátipari Tudományos Egyesület (SZTE)
Elnök · President: ASZTALOS István
1034 Budapest, Bécsi út 120.
Tel.: +36-1/201-9360 ▪ E-mail: epitoanyag@szte.org.hu
Tördelő szerkesztő · Layout editor: NÉMETH Hajnalka
Címlapfotó · Cover photo: SIMON Andrea

WWW.EPITOANYAG.ORG.HU
EN.EPITOANYAG.ORG.HU

Online ISSN: 2064-4477
Print ISSN: 0013-970x
INDEX: 2 52 50 ▪ 75 (2023) 45–xx

The detection of porous media volume using the modified Archimedes method

Masoud OSFOURI ▪ Institute of Energy, Ceramics and Polymer Technology, Faculty of Materials and Chemical Engineering, University of Miskolc
Andrea SIMON ▪ Institute of Energy, Ceramics and Polymer Technology, Faculty of Materials and Chemical Engineering, University of Miskolc

Érkezett: 2023. 04. 26. ▪ Received: 26. 04. 2023. ▪ https://doi.org/10.14382/epitoanyag-jsbcm.2023.07

Abstract
Foam glasses are novel materials in engineering that have found a special place in various industries during recent decades. Foam glass is generally produced using recycled glass. By using waste materials, in addition to reducing the amount of waste glass that can harm the environment, it is possible to achieve a lightweight foam that is resistant to compression, corrosion, and heat transfer. The foam glass structure consists of cells that are filled with gas, and the walls of these bubbles are made of solid glass. One of the challenges is to measure its density. Because the samples made in the laboratory generally do not have a conventional shape, and therefore it is difficult to find the volume of the samples geometrically. In this paper, a new, simple, and practical method to find the density of foam glass is presented. The result of the tests showed a very good coincidence between geometrical volume measurements and volumes measured by using this novel method.
Keywords: glass foam, volume, modified Archimedes method, porous materials
Kulcsszavak: üveghab, térfogat, módosított Archimédeszi-módszer, porózus anyagok

Masoud OSFOURI
is PhD student in material science and works on foam glass and light weight concrete at the University of Miskolc in Hungary. His background is mechanical engineering and his MSc thesis dealt with shape memory alloys and fiber metal laminates. He received his MSc degree in applied mechanics in 2017 at the University of Zanjan. His actual research topics are foam glasses, polymer matrix composite materials, and lightweight concrete.

Andrea SIMON
works full-time at ZF Hungary Ltd. as a supplier development engineer, and part-time at the University of Miskolc as an associate professor. She received her PhD degree in materials science and engineering in 2010 at the University of Miskolc. Her actual research topics are foam glasses, waste recycling, and microstructural characterization.

1. Introduction

Foam glass is a porous material with a glassy skeleton in which the holes are surrounded by thin glass walls and separated from each other. Foam glass has a unique combination of properties: lightweight, rigid, and strong, compression resistant, thermal insulation, non-flammable, chemically neutral and non-toxic, resistant to rodents and insects, resistant to bacteria, water, and humidity. In addition, it is easy to install, cut, and drill, and it is easily combined with concrete. This combination of properties makes foam glass indispensable in the construction and petrochemical industries (oil and gas transmission lines), railroad foundations, dam constructions, foundations of streets and highways, sports fields, and many other fields [1].

In the process of making foam glass, firstly the waste glass is ground and turned into fine glass powder. Then the powder is mixed with a foaming agent. The mixture consisting of glass powder and foaming agent is heated to a temperature at which the reaction of the foaming agent begins. The product of this reaction is gas that results in a large number of small spherical bubbles, and a cellular structure is created. After cooling, that structure forms the pores of the foam glass [2]. The properties of foamed glass products strongly depend on the type and amount of foaming agents and other additives, the particle size of the components, and the sintering conditions.

If the composition of the glass is such that it crystallizes during the production process, the possibility of the formation of closed holes will be reduced, and as a result, the quality of the final foam glass will be reduced. Therefore, the preparation of foam glass (with closed porosity) is not easily possible and requires extensive research to determine the optimal temperature of sinter-crystallization in relation to the temperature of gas exit from the material [3]. The glass softening temperature should always be lower than the foaming reaction temperature. But if the composition of the glass is prone to crystallization and the crystallization speed exceeds the sintering speed of the glass, then the crystallization of the glass will increase its viscosity, and as a result, the softening temperature of the glass will be higher than the temperature of the gas exiting the sample. In this case, the possibility of creating closed porosity in the foam glass is reduced, and open porosity increases [3, 4].

The importance of energy conservation on the one hand and the need to lighten the buildings, on the other hand, make the use of lightweight, heat, and sound-insulating but strong and stable materials in building construction more and more essential. But for being an applicable material, they require to be a low cost as well [5].

The production of foam glass dates back to the 1930s, when major research activities were carried out throughout the industrialized countries; Due to the numerous patents filed during the same period, it is not clear who were the first inventors of foam glass. The foam glass production method can be divided into two basic types, production of foam glass by sintering the above-mentioned finely ground glass powders with a suitable foaming agent and direct blowing of fluids (air, CO_2, water vapor) into molten glass [6]. Since in the research field mostly the researchers made small specimens and do different tests on them, finding the apparent volume of specimen is a big deal in the experimental research fields. There are some methods which researchers used for finding the volume of irregular shaped specimens.

In some research, they used the conventional Archimedes method for measuring the volume of irregular foam glass specimens [7-9]. When using the conventional Archimedes

method, there is inaccuracy in measuring the changed level of liquid by sinking the foam specimen. This problem leads some of the researchers to use other methods, for example a gravimetric method with using pycnometer to find the density [10-14]. The pycnometer could be used as an applicable method for finding the volume of micropores but there is a need to mill the specimen to fine powder and then use that method [11]. Thus, it is a destructive method, and it could not be useful in all the research in order to find out the foam appearance volume.

All in all, as it is clear one of the most important issues in the field of porous material research is to measure the volume of irregular shape specimens. because it becomes difficult to measure due to the porous structure and irregular shape of the samples [15]. 3D scanning is a suggested method to use in order to find the volume of irregular porous foam glass [16, 17]. Since this is a time and money consuming method, there is no report regarding use of this method in the field of foam glass volume determination. As a summary, using three-dimensional scanning methods, photography and image analysis methods, and conventional Archimedes measurement methods and finding the volume by geometrically measurement method, the researchers determine the volume and subsequently the density of the foam glass. In the case that the sample is small and its shape is irregular, the mentioned methods could be ineffective or have low accuracy [18-22]. So, there is need to establish other methods to find the volume of foam glass with high accuracy, low time and money consuming. This research is explaining a modified Archimedes' method to detect the irregular volume of foam glass in a short time, low price and very easy way.

2. Theory and methods

To introduce this method, the theory of the subject has been discussed first. The volume (V) of an irregular shape substance is required. For this purpose, firstly the mass of this substance will be measured using a scale. Let the measured mass to be m_{dry}.

Now, this substance is immersed in water. The water pressure on the surface of this substant could be calculated by considering a cubic element of the sample whose length, width, and height are dx, dy, and dh, respectively.

The pressure exerted on the surfaces of this element is normal to the surface and at any point this pressure is $p=\rho gh$ where h is the distance from the free surface of the fluid, ρ is the density of the fluid at the test temperature and g is the gravity constant.

Considering that at equal heights (h), the pressure of the fluid is constant, therefore, in the element of the *Fig. 1B* (right side), dp_x and dp_y are equal to zero, so two pressures equal to dph_2 are applied to the element in opposite directions on the $dh \times dx$ and $dh \times dy$ surfaces, which cancel out each other.

However, along the height or h direction of the element, dp_h have a value equal to $\rho g(dh)$, and considering that the height of the bottom of the element from the fluid free surface is higher than the height of the upper surface of the element from the fluid surface, therefore, the total pressure will be upwards and its value is $\rho g(dh)$.

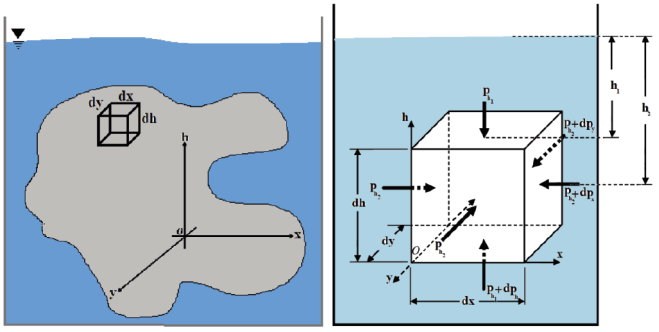

Fig. 1 The irregularly shaped object immersed in water(a) an element and hydrostatic pressure on its sides (b)
1. ábra Szabálytalan alakú tárgy vízbe merülve (a) és egy elem a hidrosztatikus nyomás jelölésével (b)

This pressure is applied on the $dx \times dy$ surface, so the amount of force corresponding to this pressure is equal to:

$$dF_b = \rho g(dh) \times dx \times dy \quad (1)$$

And the volume of this element is obtained by multiplying its lengths together, therefore:

$$dV = dh \times dx \times dy \quad (2)$$

So, *Eq. 1* can be rewritten in this way.

$$dF_b = \rho g \times dV \quad (3)$$

By taking the integral from both sides of *Eq. 3* and keeping in mind that ρg is a constant number, the upward buoyancy force applying to the object is obtained.

$$\int_V dF_b = \rho g * \iiint_V dV \Longrightarrow F_b = \rho g V \quad (4)$$

Therefore, by measuring the buoyancy force of a material in a fluid with a certain density, the volume of that material can be obtained.

Now, considering that foam glass consists of open and closed pores, it should be noted that with this method, the total volume of the foam glass solid skeleton and closed pores can be calculated. To calculate the volume of open pores, the amount of water absorption into the foam glass sample should be obtained.

To calculate the volume of foam glass, first consider a cage like in *Fig. 2*. When this cage is empty, we immerse it in water and connect it to the scale to measure the immersed weight.

In this way, weight of the floating cage in the water is obtained. Let's call this force mcage. To measure the volume of open pores of the foam glass, firstly the foam glass is boiled in water for 2 to 4 hours. This will cause the open pores to be filled with water. After this step, it should weigh the water saturated foam glass and name this weight as m_{wet}.

The volume of open pores is easily calculated through the following formula.

$$V_{Open\ porosity} = (m_{wet} - m_{dry})/\rho_{water} \quad (5)$$

Now, to calculate the volume of the skeleton and the closed pores, the water-saturated specimen is put into the cage and immersed it in the water. If the density of saturated foam glass is higher than water, then the foam will sink into the water

and the scale will show a number higher than the mcage. Otherwise, it will exert an upward force on the cage and the scale will show a number lower than the m_{cage}. In any case, we consider the number displayed by the scale as m_b.

Now, if the free graph of the foam glass and the cage is drawn (*Fig. 2-B*) and the equilibrium relations is written, the *Eq. 6* will be obtained.

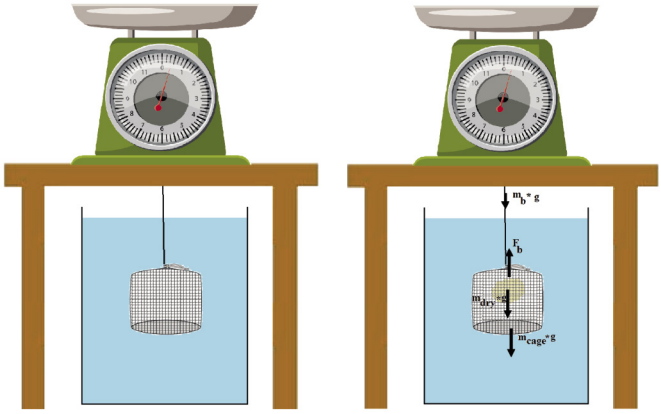

Fig. 2 Empty cage weighing in water (a). The free body diagram of the foam glass and cage in the water (b)
2. ábra Üres ketrec mérlegelése vízben (a). A vízben lévő üveghab a ketrecben (b)

$$m_b g = m_{dry}\, g + m_{cage}\, g - F_b \quad (6)$$

$$F_b = (m_{dry} + m_{cage} - m_b)\, g \quad (7)$$

By replacing the F_b obtained from *Eq. 7* in *Eq. 4* the following formulation for the volume of foam glass (skeleton plus closed porosity) is obtained. Let's call this volume V_1.

$$V_1 = \frac{m_{dry} + m_{cage} - \quad b}{\rho} \quad (8)$$

The apparent volume of foam glass is the sum of V_1 and $V_{open\text{-}porosity}$.

To check the validity of this argument, different cubic and cylindrical shapes with different dimensions were tested. The material of examined samples was made of plastic material and the samples did not absorb water. The obtained density of water was measured as 995.4 gr/lit. After the initial experiments, foam glass was made using recycled window glass and with a combination (in weight) of 1%, 2%, and 3% of silicon carbide and 1%, 2%, and 3% of alumina. In order to fabricate the samples, 4 grams of the mixture was poured into a mold with a diameter of 2.5 cm and after the cylindrical tablets were pressed, they were sintered in the furnace.

To check the density of the samples, first, their dry weight was measured, and their volume was obtained from the explained method.

3. Results and discussion

Fig. 3 show the comparison of measuring the volume of cylindrical and cubic samples by the modified Archimedes method and the geometrical measurement. As can be seen, the difference between the results of these two types of volume measurement is very small, the reason for the small difference that is observed is the measurement error. One of the most common errors can be the error in measuring the density of water. Another error is in measuring the weight of the sample because when the sample is immersed in water, the turbulence of the water can cause errors in the measurement. On the other hand, the scale used was a scale with 2 decimal digits, so it enters another error. Another error is the inaccuracy in measuring the dimensions of the samples by caliper and the asymmetry of the samples can cause errors so that there is a possibility that the examined samples are not perfectly cubic or cylindrical.

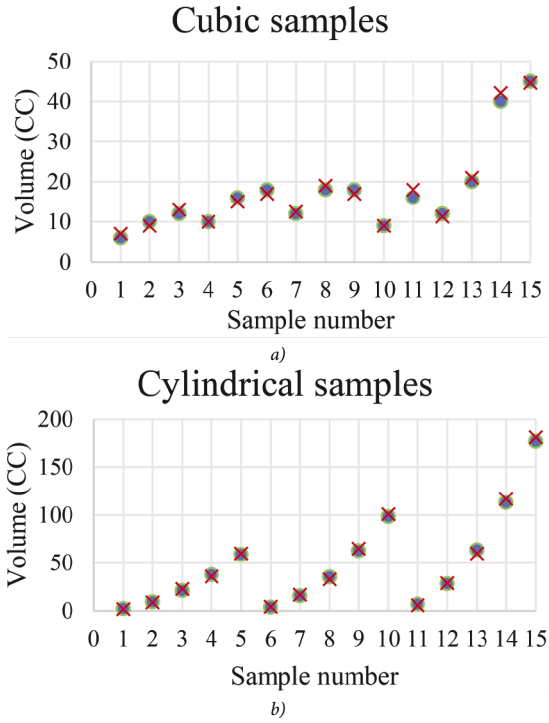

Fig. 3 The difference in obtained volume from geometrically measurement and modified Archimedes measurement in cubic (a) and cylindrical samples (b) (the red marks show data for geometrical volume and the blue marks represent the Archimedes measurements)
3. ábra A geometriai mérésből és módosított Archimedes-mérésből kapott térfogat különbsége négyzetes (a) és hengeres alakú minták esetén (b) (a piros jelek a geometriai térfogatra vonatkozó adatokat, a kék jelek pedig az Archimedes mérések eredményeit jelölik)

Sample No.	Water absorption (w%)	Open porosity volume (CC)	Foam glass volume (CC)	Expansion (V%)	Density (g/CC)
1	6.605	0.258	11.950	336.081	0.326
2	15.910	0.620	19.734	555.000	0.196
3	81.268	3.173	21.053	592.088	0.184
4	15.473	0.601	14.034	394.692	0.275
5	46.433	1.803	17.171	482.895	0.225
6	8.669	0.340	15.536	436.935	0.251
7	41.645	1.630	9.788	275.279	0.398
8	7.489	0.296	10.689	300.616	0.368
9	12.784	0.503	13.369	375.988	0.292

Table 1 Extracted data from the experiments on foam glass
1. táblázat Üveghab minták esetén végzett vizsgálatok eredményei

With all the explanations that were given, the maximum error between measuring the volume through geometry and the explained modified Archimedes method is 4%.

In the test conducted on foam glass samples, the amount of water absorption, the volume of open porosity, the percentage of volumetric expansion, and the volume and density of the samples were extracted as well. The average data for each group of samples is given in the table below (*Table 1*).

According to the results, it can be concluded that the method proposed in this research is one of the simplest methods to find the density of foam glasses precisely. This method has very low error and its accuracy is high. For using this method, fluids with lower surface tension can be used in order to better saturate the foam.

4. Conclusions

In this study, a modification of the Archimedes method was presented and discussed theoretically and experimentally in order to obtain the volume of porous materials. To measure the volume of foam, the following steps should be done:

1. A cage with a higher density than water should be provided.
2. The weight of the immersed cage in water should be measured.
3. Weight of dry foam glass or other required object which is required to find the volume.
4. The foam glass should be boiled in water for 4 hours until its open pores are saturated with water.
5. The saturated foam glass should be weighed.
6. The next step is to put the saturated object in the cage and measure the weight of the set (cage and object) as it is immersed in water.
7. Finally, the apparent volume of the object could be calculated using *Eq. 5*, *7* and *8*.

References

[1] Rabinovich E: Preparation of glass by sintering. Journal of Materials Science 1985, 20(12):4259-4297

[2] Fernandes H, Tulyaganov D, Ferreira J: Preparation and characterization of foams from sheet glass and fly ash using carbonates as foaming agents. Ceramics international 2009, 35(1):229-235. https://doi.org/10.1016/j.ceramint.2007.10.019

[3] König J, Petersen RR, Yue Y: Influence of the glass particle size on the foaming process and physical characteristics of foam glasses. Journal of Non-Crystalline Solids 2016, 447:190-197. https://doi.org/10.1016/j.jnoncrysol.2016.05.021

[4] Yatsenko EA, Goltsman BM, Smoliy VA, Kosarev AS, Bezuglov RV: Investigation of the influence of foaming agents' type and ratio on the foaming and reactionary abilities of foamed slag glass. Biosciences Biotechnology Research Asia 2015, 12(1):625-632. https://doi.org/10.13005/bbra/2242

[5] Segui P, Doré G, Bilodeau J, Morasse S: Innovative materials for road insulation in cold climates: foam glass aggregates. In: Proceedings of the 2016 Conference and Exhibition of the Transportation Association of Canada—Efficient Transportation—Managing the Demand, Toronto, ON, Canada: 2016. 22-28.

[6] Bai J, Yang X, Xu S, Jing W, Yang J: Preparation of foam glass from waste glass and fly ash. Materials Letters 2014, 136:52-54. https://doi.org/10.1016/j.matlet.2014.07.028

[7] Saparuddin DI, Hisham NAN, Ab Aziz S, Matori KA, Honda S, Iwamoto Y, Zaid MHM: Effect of sintering temperature on the crystal growth, microstructure and mechanical strength of foam glass-ceramic from waste materials. Journal of Materials Research and Technology 2020, 9(3):5640-5647. https://doi.org/10.1016/j.jmrt.2020.03.089

[8] Liu Y, Xie J, Hao P, Shi Y, Xu Y, Ding X: Study on factors affecting properties of foam glass made from waste glass. Journal of Renewable Materials 2021, 9(2):237. https://doi.org/10.32604/jrm.2021.012228

[9] Akai T, Fukumi K, Yamashita M: Formation of pale foam glass from colored glass cullet. Journal of the Ceramic Society of Japan 2020, 128(3):153-157. https://doi.org/10.2109/jcersj2.19191

[10] Paunescu L, Axinte SM, Grigoras BT, Dragoescu MF, Fiti A: Testing the use of microwave energy to produce foam glass. European Journal of Engineering and Technology Vol 2017, 5(4)

[11] König J, Petersen RR, Yue Y: Influence of the glass–calcium carbonate mixture's characteristics on the foaming process and the properties of the foam glass. Journal of the European Ceramic Society 2014, 34(6):1591-1598. https://doi.org/10.1016/j.jeurceramsoc.2013.12.020

[12] Yatsenko EA, Goltsman BM, Klimova LV, Yatsenko LA: Peculiarities of foam glass synthesis from natural silica-containing raw materials. Journal of Thermal Analysis and Calorimetry 2020, 142:119-127

[13] Mustafa WS, Nagy B, Szendefy J: Impact of compaction ratio and loading period on compressional behavior of foam glass aggregates. Construction and Building Materials 2022, 343:128111. https://doi.org/10.1016/j.conbuildmat.2022.128111

[14] Wattanasiriwech D, Nontachit S, Manomaivibool P, Wattanasiriwech S: Foam glass from municipal waste as a lightweight aggregate for cement mortar. In: IOP conference series: earth and environmental science: 2019. IOP Publishing: 012008.

[15] Corigliano A, Rizzi E, Papa E: Experimental characterization and numerical simulations of a syntactic-foam/glass-fibre composite sandwich. Composites Science and Technology 2000, 60(11):2169-2180. https://doi.org/10.1016/S0266-3538(00)00118-4

[16] Reichert J, Schellenberg J, Schubert P, Wilke T: 3D scanning as a highly precise, reproducible, and minimally invasive method for surface area and volume measurements of scleractinian corals. Limnology and Oceanography: Methods 2016, 14(8):518-526. https://doi.org/10.1002/lom3.10109

[17] Kordi M, Haralabidis N, Huby M, Barratt PR, Howatson G, Wheat JS: Reliability and validity of depth camera 3D scanning to determine thigh volume. Journal of Sports Sciences 2019, 37(1):36-41. https://doi.org/10.1080/02640414.2018.1480857

[18] König J, Petersen RR, Yue Y: Fabrication of highly insulating foam glass made from CRT panel glass. Ceramics international 2015, 41(8):9793-9800. https://doi.org/10.1016/j.ceramint.2015.04.051

[19] Hesky D, Aneziris CG, Groß U, Horn A: Water and waterglass mixtures for foam glass production. Ceramics International 2015, 41(10):12604-12613. https://doi.org/10.1016/j.ceramint.2015.06.088

[20] Song H, Chai C, Zhao Z, Wei L, Wu H, Cheng F: Experimental study on foam glass prepared by hydrothermal hot pressing-calcination technique using waste glass and fly ash. Ceramics International 2021, 47(20):28603-28613. https://doi.org/10.1016/j.ceramint.2021.07.019

[21] Nikolenko S, Sazonova S, Asminin V, Zherdev V, Ivanova V: Dust cleaning of working areas in the production of granulated foam glass ceramics. In: AIP Conference Proceedings: 2021. AIP Publishing LLC: 060030.

[22] Jaafar SH, Zaid MHM, Matori KA, Ghazali MSM, Shofri MFSM, Hisham NAN, Saparudin DI: Effect of sintering temperatures and foaming agent content to the physical and structural properties of wollastonite based foam glass-ceramics. Science of Sintering 2020, 52(3)

Ref.:
Osfouri, Masoud – **Simon**, Andrea: *The detection of porous media volume using the modified Archimedes method*
Építőanyag – Journal of Silicate Based and Composite Materials, Vol. 75, No. 2 (2023), 48–51. p.
https://doi.org/10.14382/epitoanyag-jsbcm.2023.07

Use of recycled aggregates from different sources in the production of SCC Part II: Hardened state properties

Saad CHAIB
PhD candidate, Department of Civil Engineering, University of Laghouat, Algeria. His research interests include self-compacting concrete, recycled aggregates.

Lakhdar AZZOUZ
Professor at the Department of Civil Engineering, University of Laghouat, Algeria. His research interests include reuse of local materials, concrete technology.

Benchaa BENABED
Professor at the Department of Civil Engineering, University of Laghouat, Algeria. His research interests include self-compacting concrete, rheology and durability of concrete.

Saad CHAIB ▪ Civil Engineering Research Laboratory (LRGC), University of Laghouat, Algeria
Lakhdar AZZOUZ ▪ Civil Engineering Research Laboratory (LRGC), University of Laghouat, Algeria
Benchaa BENABED ▪ Civil Engineering Research Laboratory (LRGC), University of Laghouat, Algeria
Érkezett: 2023. 04. 03. ▪ Received: 03. 04. 2023. ▪ https://doi.org/10.14382/epitoanyag-jsbcm.2023.8

Abstract
The mechanical resistance, water absorption, porosity and problems of dimensional variation due to shrinkage prove to be primordial and of great importance for evaluating of the durability of self-compacting concrete (SCC) based on recycled coarse aggregates. In part II of this study, ordinary gravel is partially replaced (50 and 100%) by recycled gravel for the preparation of eight compositions, with a constant water/binder ratio (W/B) = 0.4 and a binder dosage equal to 475 kg/m^3. Physical and mechanical properties of SCC are evaluated through a number of laboratory tests. According to the findings of this study, the water absorption and porosity of SCC with recycled coarse aggregates are generally high, and can reach up to double that of the control SCC. Shrinkage of SCC is significant, however mechanical resistance is low compared to SCC with oridinary gravel. The results also suggest that, using binary mixtures can significantly improve the durability of SCC.
Keywords: Recycled aggregates; brick; marble; bituminous aggregates; SCC, strength, water absorption, shrinkage
Kulcsszavak: újrahasznosított adalékanyagok; tégla; márvány; bitumenes adalékanyagok; SCC, szilárdság, vízfelvétel, zsugorodás

1. Introduction

SCC are very fluid concretes that flow and are placed under their own weight without the use of any internal or external energy. This fluidity is achieved by using a large amount of paste and a superplasticizer. The selection of aggregates (fine and coarse) thus plays a significant role in obtaining the best properties. To achieve a good performance-cost ratio, it is vital to have a clear grasp of the influence of physical parameters on the performance of SCC [1, 2]. Public buildings, bridges, and industrial structures are demolished but never recycled after natural disasters such as earthquakes and floods, or as a result of aging and degradation. Furthermore, natural resources in particular areas are depleted, sea sand is restricted. Therefore, aggregates are brought from long distances, and public landfills are overburdened. Unfortunately, research on waste recovery in building and public works is uncommon. Aside from the considerable shortage in aggregates encountered in recent years, demolition and building waste is significant and rarely recovered. Recycled aggregates are essentially aggregates obtained by recycling concrete from demolition. Indeed, these aggregates have different applications in the field of civil engineering, particularly in road construction and in the preparation of concrete for different buildings. In addition, the current environmental policy promotes their use with a view to reducing the consumption of raw materials and complying with environmental rules. The use of recycled aggregates in concrete [3-6], such as SCC, is hindered by many technical codification texts. Some researches have been carried out to use waste as recycled aggregates in ordinary concrete and in SCC, among these researches the study of the influence of crushed sand by Benabed [3] and the recovery of construction and demolition waste (brick and concrete in particular) by Azzouz et al. [4], Douara [5] and Nezergui [6]. In addition, the lack of knowledge about the durability of these concretes generates mistrust among the users. As a result, a better understanding of the behavior of concretes including such aggregates could aid in the development of this type of application. Hence, this project was conducted to contribute to the development of the recycling industry and the recovery of building and demolition wastes in order to use recycled gravel in the manufacture of SCC On one hand. On the other hand, to understand the primary element influencing the selection of the granular skeleton in an optimal SCC formulation. The purpose of this research is to investigate the effect of recycled gravel characteristics, types, classes, and nature on the physical and mechanical properties of SCC at hardened state. This study will contribute to the advancement of knowledge about the production of SCC by judicious choices of available gravels.

2. Materials and experiments

2.1 Materials

In this study, Ordinary Portland cement (CEM I 42.5) was used in the preparation of the various SCC mixtures, with density and specific surface areas of 3.15 and 3700 cm^2/g, respectively. A marble powder (MP) was used as mineral addition with a rate of substitution of 10%. This powder has

Properties	OCG		WMG		RBG		DCG		BMG	
Size (mm)	(3/8)	(8/16)	(3/8)	(8/16)	(3/8)	(8/16)	(3/8)	(8/16)	(3/8)	(8/16)
Absolute density	2.691	2.673	2.71	2.695	2.216	2.227	2.568	2.592	2.286	2.292
Apparent density	1.365	1.395	1.368	1.392	0.946	0.949	1.127	1.18	1.128	1.048
Compactness (%)	50.72	52.19	50.48	51.65	42.69	42.61	43.89	45.52	49.34	45.72
Porosity (%)	49.28	47.81	49.52	48.35	57.31	57.39	56.11	54.48	50.66	54.28
Water absorption (%)	2.31	1.46	0.44	0.28	10.91	9.67	8.23	5.90	1.11	1.60
Surface cleanliness (%)	0.29	0.19	0.81	0.18	0.78	0.26	1.79	1.27	0.28	0.39
Elongation coefficient	0.33	0.57	0.30	0.48	0.34	0.37	0.39	0.64	0.42	0.62
Kurtosis coefficient	0.33	0.45	0.38	0.39	0.33	0.48	0.33	0.43	0.33	0.47
Los-Angeles (%)	25.1	21.1	32.7	28.3	42.8	46.3	34.5	26.4	23.8	25.6
Micro-Deval (%)	8.2	5.2	8.1	15.6	16.1	36.8	12.9	11.2	8.4	11.9

Table 1 Properties of the aggregates used [7]
1. táblázat A felhasznált adalékanyagok tulajdonságai [7]

a density of 2.70 and a fineness of 3600 cm^2/g. A high water-reducing superplasticizer was employed. A river sand SA (0/5) of siliceous nature was used with a density of 2.65. As coarse aggregates, an ordinary crushed gravel (OCG) of limestone nature, and four types of recycled gravel: recycled gravel (GWM) produced by crushing white marble waste, recycled gravel (GRB) produced by crushing red brick waste, recycled gravel (GDC) produced by crushing demolition concrete and gravel (GBM) recycled produced by recycling bituminous mixtures. The different properties of the aggregates used are summarized in *Table 1* [7].

2.2 Testing

Nine (09) mixtures of SCC were prepared in the laboratory, in these mixtures recycled gravel was used as a substitute for ordinary gravel, with substitution rates by volume of 0, 50 and 100%. All mixtures are characterized by a powder content equal to 475 kg/m^3, water/binder (W/B) = 0.4 and sand/mortar (S/M) ratio = 0.5 [7]. Mix-proportions of the different SCC are given in *Table 2*.

From each concrete mixture, prismatic specimens 7×7×28 cm in size were cast. After casting, the specimens were unmolded and transferred to conservation at temperature of 20 ± 2 °C and 100% of relative humidity until the time of test. For each mix, three specimens were used to determine tensile strength and six specimens to measure compressive strength at 3, 7, 28, 56 and 90 days. The strength was measured according to NF P18-455 standard [8]. The density hardened SCC is determined in accordance with NF P18-435 standard [9]. While, the water absorption test was carried out in accordance with NF P 10 502 standard [10]. Drying shrinkage was carried out in accordance with NF P 18 432 standard [11].

3. Results and discussion

In the Part I of this investigation [7], the influence of the type of coarse aggregates on fresh properties of SCC was studied. The obtained results are summarized in *Table 3*.

3.1 Hardened density

The density of hardened SCC mixture is shown in *Fig. 1*. Form this figure, it is obseved that recycled gravel SCC has a low density when compared to control concrete (SCC1), with the exception of mixes containing recycled gravel from marble waste GWM (SCC2 and SCC6), which having a density similar to that of ordinary gravel (OCG). As a result, the density of

S/M = 0.5 W/B = 0.4 Constituents		Family A					Family B			
		SCC 1 100% OCG	SCC 2 100% WMG	SCC 3 100% BMG	SCC 4 100% DCG	SCC 5 100% RBG	SCC6 (50%OCG +50%WMG)	SCC7 (50%OCG +50%BMG)	SCC8 (50%OCG +50%DCG)	SCC9 (50%OCG +50%RBG)
Cement (kg/m^3)		433.7	433.7	433.7	433.7	433.7	433.7	433.7	433.7	433.7
Marble powder (kg/m^3)		41.3	41.3	41.3	41.3	41.3	41.3	41.3	41.3	41.3
Sand (kg/m^3)		901.5	872.3	916.6	937.7	960.5	883.1	901.9	914.7	920.7
Ordinary gravel (kg/m^3)	**(8/16)**	546.0	—	—	—	—	281.7	246.9	254.6	231.8
	(3/8)	270.8	—	—	—	—	139.6	122.4	126.2	114.9
Recycled gravel (kg/m^3)	**(8/16)**	—	588.3	444	451.9	350.2	285.0	247.8	243.2	212.5
	(3/8)	—	293.7	220.9	221	172.7	142.3	123.3	118.9	104.8
Water (kg/m^3)		197.0	182.9	205.6	252.8	273	193.0	202.7	228.4	240.3
Superplasticizer	**Sp (%)**	1.00	1	1	0.9	0.9	1	1	1	1
	Sp (kg/m^3)	4.8	4.8	4.8	4.3	4.3	4.8	4.8	4.8	4.8

Table 2 Mix-proportions of the different SCC [7]
2. táblázat Az öntömörödő betonok (SCC-k) keverékarányai [7]

SCC mix.		Slump flow test		J-Ring test			V-Funnel test	Sieve stability segregation test	L-Box test
		D (mm)	T500 (s)	Dj (mm)	T500J (s)	Bj (cm)	Tv (s)	π (%)	H_2/H_1 (%)
Family (A)	SCC 1	734	1.6	711	1.95	1.58	6.15	6.30	82.51
	SCC 2	722	1.85	706	2.25	1.88	6.90	6.90	80.60
	SCC 3	765	0.95	728	1.25	1.43	5.30	18.65	90.36
	SCC 4	697	1.9	688	2.20	1.08	7.35	9.68	93.70
	SCC 5	682	1.95	663	2.40	2.03	7.10	10.15	78.23
Family (B)	SCC 6	732	1.85	698	2.05	1.67	6.65	7.38	86.10
	SCC 7	728	1.35	704	1.90	1.64	5.85	15.28	83.67
	SCC 8	739	1.75	712	1.95	1.18	6.90	8.96	90.20
	SCC 9	717	1.70	681	2.10	1.86	6.85	10.28	80.33

Table 3 Fresh properties of SCC made with different types of coarse aggregates [7]
3. táblázat Különböző típusú durva aggregátumokkal készült öntömörödő betonok (SCC) friss tulajdonságai [7]

SCC with recycled coarse aggregates is often lower than that of the reference SCC (SCC1 with 100% OCG). The figure also shows a general increase in the density of concrete of family B compared to recycled SCC in family A, which is due to a reduction in the amount of recycled gravel (100%, 50%), because these SCC contain 50% OCG gravel, which has a higher density than recycled gravel.

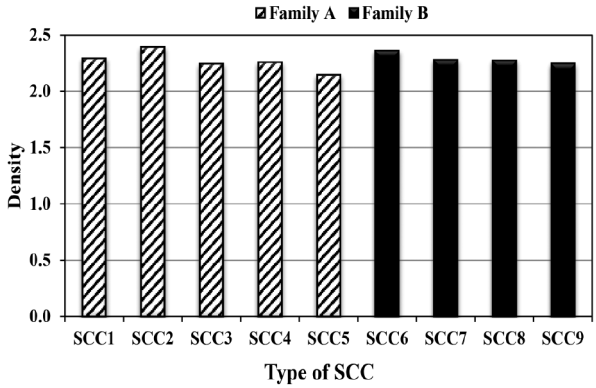

Fig. 1 Haredened density of the different SCC mixtures
1. ábra Az öntömörödő betonkeverékek (SCC) szilárdulás utáni sűrűsége

3.2 Compressive strength

The *Fig. 2* and *3* depict the evolution of compressive strenght of different SCC made with the different types of recycled aggregates. The strength of all mixes increases with age. It should be emphasized that the compressive strength of SCC made with recycled gravel changes over time in the same way that SCC1 does; however, it decreases depending on the proportion of substitution in recycled gravel.

At 28 days, the resistance of the combinations SCC2, SCC3, SCC4, SCC5, SCC6, SCC7, SCC8, and SCC9 decreased by 5, 46, 16, 39, 9, 24, 10, and 18%, respectively, as compared to the reference mixture (SCC1). As a result, the maximum compressive strength after 28 days is attained in the reference concrete SCC1 and is equivalent to 39.54 MPa, but the loss in strength at 28 days of recycled SCC mixes is of the order of 5 to 46% when compared to SCC1. It is observed that, the compressive strength values in the medium and long term of mixtures made from OCG and GWM gravel (SCC1 and SCC2), as well as the mixture of two types of these SCC6 gravel, are higher than the other values of mixtures based on recycled gravel. This can be explained by the fact that the strength of the concrete is influenced by the texture and shape of coarse aggregates. As a result, the adhesion strength between OCG and GWM and the cement paste is stronger than that of recycled gravel.

With regard to the binary mixtures of the family B (contain 50% OCG), a reduction in resistance was noted compared to SCC1. For SCC7, the reduction in resistance is primarily due to an increase in the W/B ratio and the effect of the mortar of the old inert concrete which is attached to the gravel coming from the crushed concrete, which hinders the good progress of the cement hydration [12]. For SCC8, the reduction in resistance is primarily due to the crushed brick gravel which has a high water absorption. For SCC9, this reduction in resistance is related to the bitumen that covers the grains of coarse aggregates. The lowest compressive strength at 28 days is attained in SCC3 (100% GBM) and is 21.18 MPa. This decrease can be due to bituminous gravel (GBM), which is less stiff than other gravel and, when compressed, will crush and slide against one other rather than resisting the compression. Benabed [13] demonstrated that the resistance of SCC after hardening is affected by the W/B ratio, the quality and type of the aggregates, the technique of conservation, and the test expiration date. Pandaa and Balb [14] have shown that the compressive strength of SCC diminishes as the rate of recycled coarse aggregates increases. According to Persson [15], the compressive strength difference between SCCs and regular concrete is 20 MPa and 5 MPa for water/binder ratios W/B = 0.4 and 0.5, respectively.

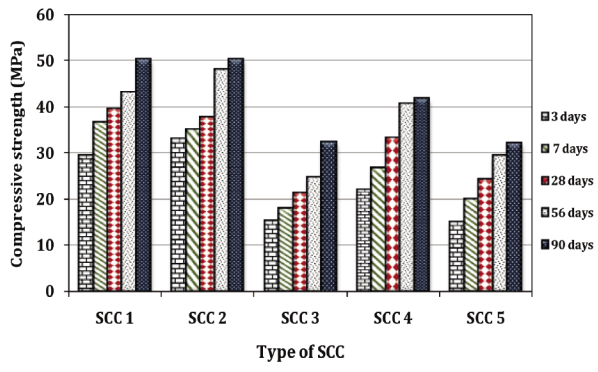

Fig. 2 Compressive strength of SCC mixtures (family A)
2. ábra Az öntömörödő betonkeverékek (SCC) nyomószilárdsága (A minták)

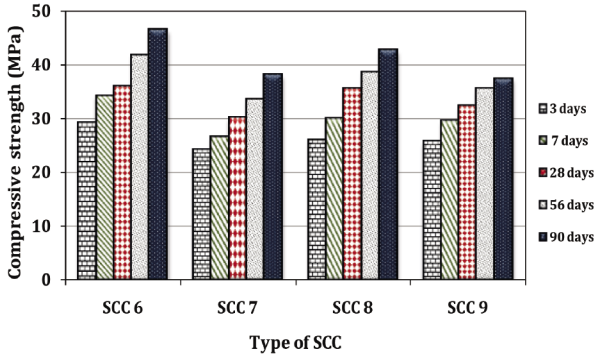

Fig. 3 Compressive strength of SCC mixtures (family B)
3. ábra Az öntömörödő betonkeverékek (SCC) nyomószilárdsága (B minták)

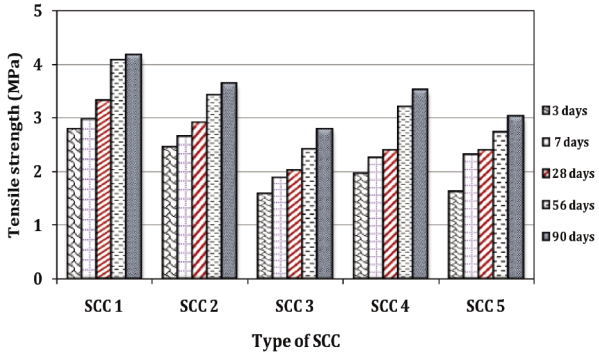

Fig. 4 Tensile strength of SCC mixtures (family A)
4. ábra Az öntömörödő betonkeverékek (SCC) szakítószilárdsága (A minták)

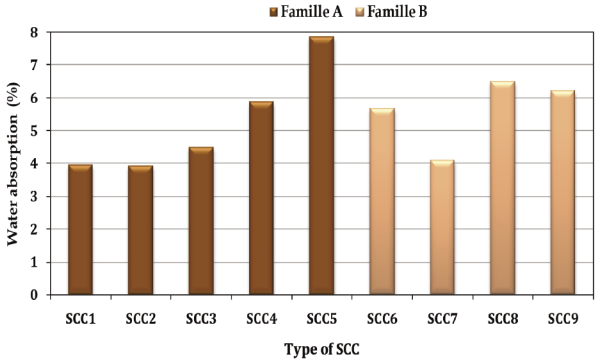

Fig. 5 Tensile strength of SCC mixtures (family B)
5. ábra Az öntömörödő betonkeverékek (SCC) szakítószilárdsága (B minták)

3.3 Tensile strength

Fig. 4 and *5* show the tensile strength results of all mixtures, which showed the same tendency as the compressive strength. Tensile strength diminishes as the fraction of recycled coarse aggregates increases from 50% to 100%. At 28 days, the SCC1, SCC2, and SCC6 combinations have the highest tensile strength values, which are 3.32, 2.90, and 2.92 MPa, respectively. This rise is explained by the substantial roughness of the surface of the OCG and GWM gravel particles. The flexural strength of the combinations including crushed aggregates improved. This is explained by the angularity of the gravel grains, which ensures good adhesion between the grains and the cement matrix in one hand. In the other hand by the presence of micro-fines filling the micropores, which allows densification of the cement paste microstructure [16]. The addition of coarse bituminous aggregates to the various SCC combinations (SCC3 and SCC7) reduces the bearing capacity of the materials, as seen in *Fig. 4* and *5*. This drop can be attributed to poor adhesion between the cement paste and the gravel grains of asphalt mixes as a result of the bitumen that covers the grains of (GBM) and the cement paste, resulting in a low tensile strength.

3.4 Water absorption by immersion

Fig. 6 shows that water absorption of different mixtures of SCC. It can be seen that the water absorption of greater SCC mixtures with recycled gravel (excluding SCC2) are higher than for the control concrete SCC1 of ordinary gravel (OCG). When the degree of substitution in recycled gravel increases, the percentage of water absorption increases up to 2 times (SCC5). The proportion of substitution in recycled gravel (50% or 100%) increases the water absorption of recycled SCC. Because of its gravel (GRB), which has a higher water absorption coefficient than other gravel, recycled SCC prepared with crushed brick gravels (SCC5 and SCC9) are somewhat more permeable than other recycled concretes and have water penetration that can exceed double that of the reference concrete. It may be concluded that the nature and percentage of recycled gravel have a substantial influence on water absorption by immersion of recycled SCC. According to Topcu et al. [17], a decrease in concrete density is accompanied by an increase in air volume, which diminishes the compactness and, as a result, increases the porosity of the mixture.

3.5 Water absorption by capillary

Fig. 7 depicts the variation of water absorption by capillary of the various SCC. It is noticed that the type of gravel has a major influence on the capillary absorption of SCC. SCC5 has the highest capillary absorption value of any mixture; it absorbs more than other mixtures due to its crushed brick gravel (GRB), which has a greater water absorption coefficient than other gravel (Abs 10%). Because of the presence of mortar on the grains, the grains of (GRB), which are totally crushed materials, have very angular forms, have a rougher surface, lower density, and greater capillary absorption than gravel grains (OCG). The density falls and the absorption increases correspondingly as the grain size of (GRB) lowers (Fraction 8/16 minimal fraction 3/8), due to the increasing proportion of mortar adhering or which constitutes the grains of minimal fraction.

Capillary absorption is reduced when bituminous mixtures are used as 100% coarse particles (SCC3). This is owing to bitumen's hydrophobic nature, which interferes with water absorption [18], so the cement matrix is more absorbent whereas bitumen-coated (GBM) grains are hydrophobic. The high water absorption values of SCC based on recycled coarse aggregates are a proper indication of this form of SCC high porosity and permeability, and therefore of the negative influence of using these recycled gravels on the durability of the concretes. SCC mixes made with recycled gravel, in general, have a higher water absorption capacity than control concrete (SCC1). This is certainly related to the huge number

of capillary holes by volume. Water is one of the most sensitive elements affecting the characteristics of concrete, according to extensive study. Water has various significant roles in this, including hydration of cement grains, flexibility of fresh concrete, and internal cohesiveness of fresh concrete [19].

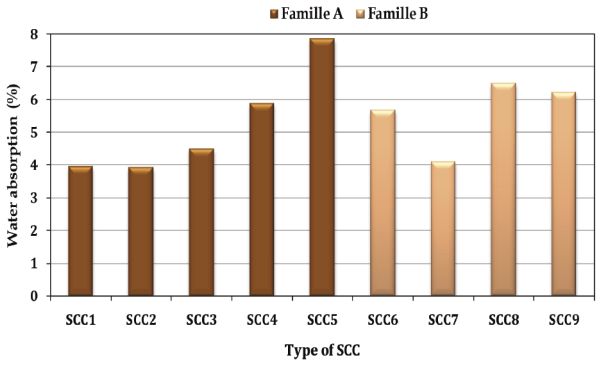

Fig. 6 Water absorption by immersion of SCC mixtures
6. ábra Az öntömörödő betonkeverékek (SCC) vízfelvétele vízbe merítéssel

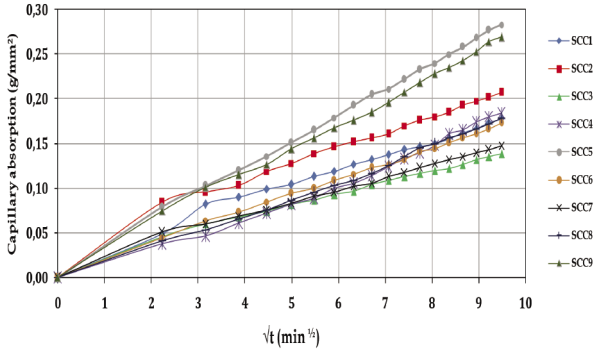

Fig. 7 Water absorption by capillarity of SCC mixtures
7. ábra Az öntömörödő betonkeverékek (SCC) kapilláris vízfelvétele

3.6 Shrinkage

Fig. 8 shows shrinkage of the different SCC. It can be noted that SCC made entirely of recycled gravel is much greater than that of the reference concrete SCC1 made entirely of conventional gravel. This figure also reveals that the maximum shrinkage of SCC3 based on bituminous mixes (GBM) is 36% more than that of SCC1 at 28 days, increasing to 43% at 120 days. This is mostly due to the bitumen that covers the grains of this gravel acting as a water store, compensating for the drying of the cement paste for a period. The shrinkage process does not begin until all of the water trapped inside this gravel has evaporated. The shrinkage of SCC made with crushed brick gravel (GRB) is more than that of SCC1 and grows by 26% at 28 days of age; after that, it eventually increases to 23% at 120 days. The shrinkage of SCC4 contains crushed concrete gravels (GDC) is higher than that of SCC1 and reaches an increase of 8% at 120 days. This substantial shrinkage is most likely owing to the high porosity of recycled gravel as well as the high degree of water absorption of the mortar that covers the gravel. Kenai and Debieb [8] discovered that open-air concrete mixes based on crushed concrete gravel and crushed brick gravel shrink more than control concrete based on natural aggregates. Concerning the last two groups of concretes produced (SCC8 and SCC9), which are based on a binary mixture of gravel of 50%OCG + 50%GDC and 50%OCG + 50%GRB, they generally present with a delayed withdrawal compared to SCC1 from an early age, with an average decrease of 33% - 41% that can reach 13% -15% at 120 days. Shrinkage issues are significantly more likely in SCC made with recycled gravel, due to the additional water consumption during manufacturing. Only after the whole evaporation of the amount of water trapped within these gravels does shrinking occur. As a result, intelligent selection of superplasticizer type and percentage can lead to a reduction in concrete shrinkage [12], and so the addition of a superplasticizer minimizes the shrinkage of recycled SCC.

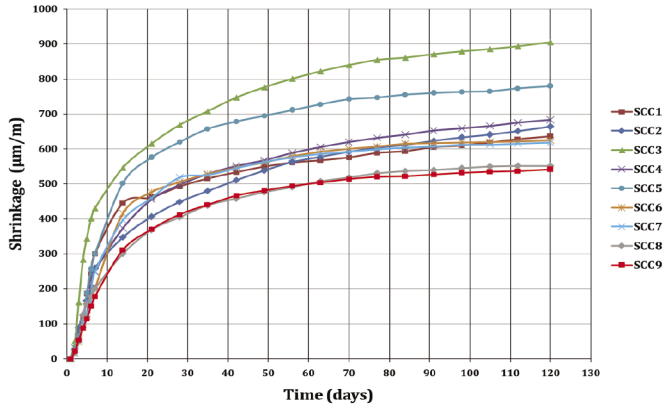

Fig. 8 Evolution of shrinkage during open-air curing of SCC
8. ábra A zsugorodás alakulása az Az öntömörödő betonok (SCC) szabadlevegőn történő szilárdulása során

4. Conclusions

The results of this work can lead to the following conclusions:

- Depending on the type of gravel, it is found that the control SCC of ordinary crushed gravel (OCG) and the SCC of crushed marble waste (GWM) have fairly similar characteristics at the hardened state. The findings show that gravel (GWM) can be technically used as a substitute in SCC.
- The compressive and tensile strength of SCC made with different types of recycled gravel increase proportionally with time, although the rate of change is not similar for the different mixtures. The obtained strengths are acceptable compared to those of the reference SCC based on ordinary gravel.
- The maximum values of mechanical strength at 28 days are obtained for SCC with 100% ordinary crushed gravel (OCG). All the tests carried out show unequivocally that the incorporation of recycled gravel (except GWM) is very detrimental to the mechanical resistance of SCC, which decreases with the increase in the dosage of recycled gravel substitution.
- The study of the influence of recycled gravel on shrinkage has shown high shrinkage at young. The higher shrinkage is achieved by the composition of SCC of 100% asphalt mix gravel (GBM). In practice, in a hot climate, this type of increase in concrete shrinkage can

be detrimental to its use in structural elements sensitive to cracking such as slabs and walls.

- The water absorption of SCC made from recycled gravel is higher than that of a control SCC made from 100% ordinary crushed gravel (OCG) and can reach double that of the control SCC. The high water absorption of recycled SCC is due to the high porosity of recycled gravel (GRB and GDC) which induces the addition of a large quantity of water to guarantee acceptable flowability. In terms of porosity accessible to water, a strong increase is observed with the increase in the proportion of recycled gravel. In addition, this is linked to the presence of the old mortar on the surface of recycled aggregates (GDC) and the material of clayey origin which makes up large aggregates (GRB).
- Replacing ordinary gravel with partially or totally recycled gravel in concrete offers a new source of supply and saves materials and quarries. Therefore the possibility of using waste gravel in SCC, as recycled gravel reduces environmental pollution and provides economic value for waste, There is also a significant growth potential of recycled aggregate as an appropriate solution for sustainable development in the construction industry.

Acknowledgements

The authors gratefully acknowledge the Directorate-General of Scientific Research and Technological Development of Algeria (DGRSDT) for its valuable support.

References

[1] Okamura H., Ozawa K. (1994) Self-compactable high performance concrete in Japan. ACI International Workshop on high Performance Concrete, Bangkok, Thailand

[2] Boukhelkhal A., Azzouz L., Belaïdi A., Benabed B. (2016) Effects of marble powder as a partial replacement of cement on some engineering properties of SCC. Journal of Adhesion Science and Technology. 30(22), 2405–2419. https://doi.org/10.1080/01694243.2016.1184402

[3] Benabed B., Kadri E., Azzouz L., Kenai S. (2012) Properties of SCC made with various types of sand", Cement and Concrete Composites. 34 (10), 1167-1173. https://doi.org/10.1016/j.cemconcomp.2012.07.007

[4] Azzouz L., Bouhicha M., Kenai S. (2001) Valorisation and recycling of brick wastes in sand concrete. Magazine of Laghouat University. Vol.3. N°1

[5] Douara T.H. (2008) Influence of additions on the quality of concrete based recycled aggregates. Msc thesis. ENSET Oran

[6] Nezergui B. (2008) Comparative study on the formulation of SCC based recycled and ordinary aggregates. Msc thesis, ENSET Oran

[7] Chaib S., Azzouz L., Benabed B. (2022) Use of recycled aggregates from different sources in the production of SCC Part I: Mix design and fresh properties. Epitoanyag-Journal of Silicate Based & Composite Materials. 74(5), 210-217 https://doi.org/10.14382/epitoanyag-jsbcm.2022.30

[8] NF P18-455 standards (2006) Hardened concrete testing: Determination of strength

[9] NF P18-435 standard (2001) Hardened concrete testing: Bulk density of concrete

[10] NF P 10 502 standard (2001) Hardened concrete testing: Water absorption by capillary

[11] NF P 18 432 standard (2001) Hardened concrete testing: shrinkage tests

[12] Kenai S., Debieb F. (2011) Characterization of the durability of recycled concretes using coarse and fine crushed bricks and concrete aggregates. Materials and Structures. 44, 822-823. https://doi.org/10.1617/s11527-010-9668-7

[13] Benabed B. (2014) Influence of sand type on performance and durability of SCC" PhD Thesis. University of Laghouat

[14] Pandaa K.C Balb P.K. (2013) Properties of self-compacting concrete using recycled coarse aggregate. Procedia Engineering 51, 159 – 164

[15] Persson B. (1999) Creep, shrinkage and elastic modulus of SCC. Proceedings of First International RILEM Symposium on SCC, Edited by Å. Skarendahl and Ö. Petersson, Stockholm, Sweden, 239 – 250

[16] Tang W.C., Ryan P.C., Cui H.Z., Liao W. (2016) Properties of SCC with Recycled Coarse Aggregate. Advances in Materials Science and Engineering. 2761294, 11 pages. http://dx.doi.org/10.1155/2016/2761294

[17] Topcu I.B., Bilir T., Uygunoglu T. (2009) Effect of waste marble dust content as filler on properties of SCC. Construction Building Materials. 23(5), 1947–1953. https://doi.org/10.1016/j.conbuildmat.2008.09.007

[18] Moniz C., Pierre P., Pleau R., Juneau S. (2013) Determination of the laboratory performance of recycled materials used in road foundations. Final report submitted to the Ministry of Transport, Québec

[19] Larrard F. (2000) Granular structures and concrete formulations. Laboratoire Central des Ponts et Chaussées, Paris

Ref.:
Chaib, Saad – **Azzouz**, Lakhdar – **Benabed**, Benchaa: *Use of recycled aggregates from different sources in the production of SCC. Part II: Hardened state properties*
Építőanyag – Journal of Silicate Based and Composite Materials, Vol. 75, No. 2 (2023), 52–57. p.
https://doi.org/10.14382/epitoanyag-jsbcm.2023.08

Scheffe optimization of the California Bearing Ratio of a kaolin blended lateritic soil for pavement construction

Chidozie Chimereze IKPA ▪ Civil Engineering Department, Alex Ekwueme Federal University Ndufu-Alike, Ikwo, Ebonyi State, Nigeria ▪ ikpa.chidozie@funai.edu.ng

Charles Chinwuba IKE ▪ Civil Engineering Department, Enugu State University of Science and Technology, Agbani, Enugu State, Nigeria ▪ Charles.ike@esut.edu.ng

George Uwadiegwu ALANEME ▪ Civil Engineering Department, Kampala International University, Uganda ▪ alanemeg@kiu.ac.ug

Érkezett: 2023. 02. 27. ▪ Received: 27. 02. 2023. ▪ https://doi.org/10.14382/epitoanyag-jsbcm.2023.9

Abstract

Improvement of the mechanical behavior of problematic lateritic soil using naturally occurring materials that can be sourced within our immediate environment has been understudied over the years due to the availability and predominance of Portland Limestone Cement (PLC) as a readily available stabilization agent. Therefore, this study presents an approach to the use of Scheffe's optimization method to model the California bearing ratio (CBR) properties of problematic lateritic soil blended with kaolin in its natural state for pavement construction purposes. A Scheffe simplex lattice second-degree polynomial was applied in formulating the model for predicting the CBR behavior of the kaolin treated laterite soil. If the mix ratio is known, the soil's said property can be predicted. A maximum CBR value of 76.6% (Y_2) was recorded for the stabilized soil sample. The Scheffe model that was used in the study of CBR behavior has been found to be adequate at a 95% confidence level. The adequacy of the model was checked using the student T-test and analysis of variance (ANOVA) test, and the model is said to be satisfactory at the same level of adequate. With the optimization model developed, the CBR behavior of soil samples with similar geotechnical properties and stabilization agents can be monitored.

Keywords: lateritic soil, stabilization, CBR, geotechnical, optimization model
Kulcsszavak: lateritikus talaj, stabilizáció, CBR, geotechnikai, optimalizálási modell

Chidozie C. IKPA
currently works at the Civil Engineering department Laboratory of Federal University Ndufu Alike Ikwo, Ebonyi state as a Research Engineer. He does research in Civil Engineering with various works on the use of industrial, agricultural, and household solid waste materials for use as admixtures and soil stabilizers. He's a registered engineer under the Council for Regulation of Engineers in Nigeria (COREN) and passionate about green construction.

Dr. Charles C. Chinwuba IKE
is an Associate Professor at the department of Civil Engineering of the Enugu State University of Science and Technology, Agbani, Enugu State, Nigeria. He is a member of the Nigerian Society of Engineers (NSE) and the Council for the Regulation of Engineering in Nigeria (COREN). He has numerous publications in conference proceedings as well as in reputable international journals on structural analysis, structural mechanics, and structural engineering. His research interests include the theory of elasticity, soil-structure interactions, theories of plates, integral transform methods, finite element methods, and nonlinear analysis.

Goerge U. ALANEME
is an Assistant Lecturer in the department of Civil Engineering at Kampala International University, Kampala with a good command of the required software programs used in automated design, analysis, and optimization. He has extensive experience in the design of linear, nonlinear, and discrete optimization problems as well as working knowledge of algorithm development and its application to solving civil engineering problems. He's a registered engineer under the Council for Regulation of Engineers in Nigeria (COREN).

1. Introduction

Over the years, researchers have developed and investigated efficient means of utilizing both agricultural and natural products to combat soil instability problems. One type of natural product that remains untapped with the potential to serve as a stabilization agent due to its binding property is kaolin. Kaolinite is formed by the weathering or hydrothermal alteration of aluminosilicate minerals. Thus, feldspar-rich rocks commonly weather to kaolinite. To form, ions like Na, K, Ca, Mg, and Fe must first be leached away by the weathering or alteration process. Kaolin serves an important function in the cement industry when highly calcinated; pulverized Kaolin adds comprehensive strength, flexural strength, and water permeability to cement [1-2].

It can be considered an interesting area for research to ascertain its optimal applicability in the stabilization of lateritic soil. Its water permeability characteristic is useful in prolonging the durability of concrete and reducing weakening. Kaolin adds flexibility, which is often preferred to the usually brittle finished product. High-performance concrete (cement with Kaolin additives) can be modified to meet a variety of applications. Its shrinkage strength when compressed and water permeability make high-performance concrete useful for pavement construction purposes, among other purposes [3].

Mathematical prediction models can be very useful tools for making informed decisions and predicting future outcomes. However, it's important to use them in conjunction with other sources of information and to be aware of their limitations and potential biases. Mathematical prediction models are very crucial in civil engineering especially in laboratory works because they help in minimize time and cost to find the properties of mixes and determine the optimum amount of additives [4, 5].

According to Usoh *et al.* [6], a mathematical model and numerical simulation of heavy metal transport in a municipal solid waste (MSW) dumpsite in Akwa Ibom State, Nigeria was developed using a two-dimensional finite element model. The results of the study showed that the transport of heavy metals in the dumpsite is influenced by several factors, including the type of heavy metal, the soil properties, and the rainfall. The study also showed that the numerical model was able to accurately simulate the transport of heavy metals in the dumpsite. Several other studies on the development of mathematical prediction models for engineering purposes have over the years also be published in various journals all over the world. These prediction models have farther been developed from just mathematical models to artificial intelligence aided models.

This study aims to find the best mixture design for pavement construction purposes by optimizing the CBR of weak lateritic soil using the Scheffe simplex lattice method by

- First ascertaining the aggregates' physical characteristics.
- Establish the ideal Kaolin content for the mix.
- Create a mathematical model that can accurately predict the California Bearing Ratio (CBR) of the blended soil sample under study.

Scheffe models were specifically developed to handle the natural constraints of mixture designs. Bearing in mind the loopholes in the trial-and-error method of choosing a working mix design, there's always a great need to subject such projects as this, requiring the mixture of three-component samples at varying proportions, to an optimization model to obtain the best mixture formula; hence, the application of the Scheffe optimization model. It was developed in 1963 for the assessment of the response of a particular characteristic of a mixture to variations in the proportions of its component materials [7, 8].

Some of the applications of Scheffe mix design includes.

1. Concrete Mix Design: Scheffe's mixture design method can be used to optimize the composition of concrete mixes, including the selection, and proportioning of different cementitious materials, aggregates, and other additives, to achieve the desired properties and performance [9].
2. Asphalt Mix Design: Scheffe's mixture design method can also be applied to optimize the composition of asphalt mixes, including the selection, and proportioning of different aggregates, asphalt binders, and additives, to achieve the desired performance characteristics such as stability, durability, and resistance to deformation [10].
3. Soil Stabilization: Scheffe's mixture design method can be used to optimize the composition of soil stabilization mixtures, including the selection, and proportioning of different soil types, binders, and other additives, to improve the strength and stability of the soil for various geotechnical engineering applications [11].
4. Composite Materials: Scheffe's mixture design method can also be applied to optimize the composition of composite materials used in civil engineering applications, including fiber-reinforced composites, polymer composites, and other types of advanced materials, to achieve the desired properties and performance [12].

Ambrose *et al* [13] investigated the effect of crushed recycled-ceramic tiles (CRT) fine aggregate content on the compressive strength of concrete. The authors found that the incorporation of CRT as fine aggregate improves the compressive strength of concrete, and this increase is directly proportional to its content. The authors also developed Scheffe's second-degree polynomial models to predict the compressive strength, slump height, and cost of CRT concrete. The models were found to be adequate at 95% confidence level. A. O. Ogunsanwo *et al* [14] in the Application of Scheffe Optimization Models on Soil Stabilization used Scheffe models to optimize the mix proportions of cement and lime for stabilizing a tropical clayey soil found that the Scheffe models were able to predict the strength and durability of the stabilized soil with a high degree of accuracy. Furthermore, Ogunsanwo *et al* [15] reviewed the application of Scheffe models on soil stabilization and concluded that Scheffe models are effective tools for optimizing the mix proportions of stabilization materials. They also recommended that more research be done on the application of Scheffe models on soil stabilization. Scheffe model was also applied in the stabilization of Amuro-okigwe subgrade using male inflorescence of oil palm ash (MIPA) [16]. They used Scheffe's model to optimize the mix proportions of MIPA and soil. They found that the optimum mix proportion of MIPA was 10.5%, which resulted in a significant improvement in the strength and durability of the soil.

2. Materials and method

2.1 Mathematical modelling and formulation of mix proportions

2.1.1 The Scheffe Model

Scheffe is an advanced system of regression analysis derived from Response Surface Methodology (RSM) through hard computing algorithms. In Scheffe's mixture optimization model, the goal is to find the optimal combination of ingredients in a mixture that will result in the desired response or outcome. This can be applied in various fields such as engineering, pharmaceuticals, food science and industrial manufacturing [17]. The model involves creating a design matrix that represents different combination of mixture components and conducting experiments to measure the response variable for each combination [18]. These measurements are then used to estimate the parameters of RSM which describes the relationship between the mixture components and the response variable. Using the estimated RSM, Scheffe's method allows for the determination for the optimal combination of mixture components that maximizes the response variable, while taking into account any constraints or limitations. The technique typically involves the use of mathematical optimization algorithms to search for the optimal solution within the defined parameter space [19]. RSM involves three major steps, which are:

i. The design of the experiment,
ii. formulation of model equations, and
iii. optimization of the equations under certain given constraints.

2.1.2 Scheffe's simplex Lattice method:

A simplex is defined as a convex polyhedron with $(k + 1)$ vertices produced by k intersecting hyperplanes in k-dimensional space. While an ordered arrangement consisting of a uniformly spaced distribution of points on a simplex is known as a lattice. Studying a mixture of n-components mixture which are dependent on the component ratio only, the factor space is a regular $(q\text{-}1)$ simplex and for the mixture the following relationship holds [20].

$$\sum_{i=1}^{q} X_i = 1 \quad (1)$$

Where: q= No of components and $X_i \geq 0$ = concentration of component.

If $q = 2$, we have the lattice simplex as a straight line, for $q = 3$, it is an equilateral triangle while for q= 4, the simplex will be a regular tetrahedron with each vertex representing each of the components. Scheffe considered experiments with mixtures,

in which the property studied depends on the proportions of the components but not their quantities in the mixture. He introduced polynomial regression to model the response, called "*q, n*-polynomial." Note that these polynomials must be of lower degree, otherwise they will be complex to interpret [21].

Note that this polynomial must be of lower degree, otherwise it will be complex to interpret. Scheffe used a regular (*q-1*) simplex to represent a factor space to describe a response surface for mixtures consisting of several components. If the number of components is denoted by *q*, then for binary system ($q = 2$) the required simplex is a straight line; for $q = 3$, the required simplex is an equilateral triangle; and for $q = 4$, the simplex is a regular tetrahedron [22]. The proportions used for each factor have $m + 1$ equally spaced levels from 0 to 1 ($x_1 = 0$ 1/m, 2/m……1), and all possible combinations are derived from such values of the component concentrations. This implies that all possible mixtures with these proportions are utilized. Hence, for the quadratic lattice (q, 2), approximating the response surface with the second-degree polynomials ($m = 2$), the following levels of every factor must be used 0, ½ and 1 [23, 24]. The number of runs *N* in a mix design can be calculated thus

$$N = \frac{(q+m-1)!}{m!(q-1)!} \quad (2)$$

Where: q = No of components present in the mix = 3

M = Desired degree of polynomial = 2

Therefore, $N = \frac{(3+2-1)!}{2!(3-1)!} = \frac{4!}{2!2!} = 6$

Mix components are assumed to interact within a factor space. The research is comprised of a 3-component mixture (soil, Kaolin, and water), which was analyzed using a triangle simplex lattice having a 2-dimensional factor space. The triangular simplex components are illustrated in *Fig. 1*.

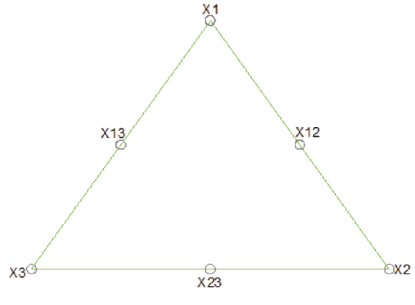

Fig. 1 Three component mixture in a three-dimensional factor space showing six points of observation
1. ábra Három komponensű keverék egy háromdimenziós tényezőtérben, amely hat megfigyelési pontot mutat

2.1.3 Pseudo and actual components

Pseudo-components are imaginary or coded variables used to simplify design construction and model fitting, thereby reducing the correlation between component bounds in constrained designs. Scheffe provided an equation for elucidating the relationship between the pseudo component(x) and the actual component (z) in their mixture designs [25]. The summation of the pseudo components must be equal to unity as written in *Eq.4*

$$Z = AX \quad (3)$$

$$0 \leq x_1 \leq 1 \quad (4)$$

According to (9) Z represents the actual components while X represent the pseudo components, where A is the constant; a three-by-three matrix for the present work under study. The value of matrix A will be obtained from the three mix ratios. The mix ratios which are the actual components at the vertices are chosen at random with the key component being optimized kept at a constant value not more than unity [26].

A being a matrix of coefficient.

Therefore $X = ZA^{-1}$ (5)

From the actual components Z, a three-by-three matrix is formed which when transposed becomes a conversion factor from the pseudo to real components. Assuming we select the first three mix rations as; thus, $Z_1(A_{11}, A_{21}, A_{31},)$, $Z_2(A_{12}, A_{22}, A_{32},)$, $Z_3(A_{13}, A_{23}, A_{33},)$ then the actual component simplex is shown below.

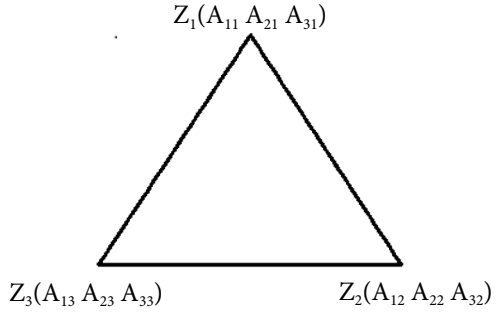

Fig. 2 Simplex components at vertices only
2. ábra Szimplex komponensek csak csúcsokban

With a 3 by 3 matric of

$$\begin{vmatrix} A_{11} & A_{21} & A_{31} \\ A_{12} & A_{22} & A_{32} \\ A_{13} & A_{23} & A_{33} \end{vmatrix} \quad (6)$$

When transposed becomes

$$Z^T = \begin{vmatrix} A_{11} & A_{12} & A_{13} \\ A_{21} & A_{22} & A_{23} \\ A_{31} & A_{32} & A_{33} \end{vmatrix} \quad (7)$$

Furthermore, the actual components along the vertices can be gotten by substituting the required data into *Eq. 8*

$$\begin{bmatrix} Z_1 \\ Z_2 \\ Z_3 \end{bmatrix} = \begin{vmatrix} A_{11} & A_{12} & A_{13} \\ A_{21} & A_{22} & A_{23} \\ A_{31} & A_{32} & A_{33} \end{vmatrix} \begin{bmatrix} X_1 \\ X_2 \\ X_3 \end{bmatrix} \quad (8)$$

The value of A derived from the first three mix ratios. The mix ratios are.

$Z_1(1.00, 0.25, 0.15)$, $Z_2(1.00,0.55,0.16)$, $Z_3(1.00,0.75,0.17)$, with corresponding pseudo mix ratios in the form of an identity matrix which signifies that these points lie on the vertices of the simplex; thus, $X_1(1, 0, 0)$, $X_2(0,1,0)$, $X_3(0,0,1)$.

Substitution of X_i^{th} and Z^{ith} into *Eq. 8*, then the corresponding pseudo components are used to determine the corresponding actual mixture components. However, X_1 equals proportion of sample soil, X_2 equals proportion of kaolin, and X_3 equals proportion of water [27, 28].

For the first run:

$$\begin{bmatrix}1\\0.25\\0.15\end{bmatrix} = \begin{bmatrix}A_{11} & A_{12} & A_{13}\\A_{21} & A_{22} & A_{23}\\A_{31} & A_{32} & A_{33}\end{bmatrix}\begin{bmatrix}1\\0\\0\end{bmatrix} \quad (9)$$

a_{11}= 1.0, a_{21}= 0.25, a_{31}= 0.15

For the second run

$$\begin{bmatrix}1\\0.55\\0.16\end{bmatrix} = \begin{bmatrix}A_{11} & A_{12} & A_{13}\\A_{21} & A_{22} & A_{23}\\A_{31} & A_{32} & A_{33}\end{bmatrix}\begin{bmatrix}0\\1\\0\end{bmatrix} \quad (10)$$

a_{12}=1.0, a_{22}= 0.55, a_{32}= 0.16

For the third run

$$\begin{bmatrix}1\\0.75\\0.17\end{bmatrix} = \begin{bmatrix}A_{11} & A_{12} & A_{13}\\A_{21} & A_{22} & A_{23}\\A_{31} & A_{32} & A_{33}\end{bmatrix}\begin{bmatrix}0\\0\\1\end{bmatrix} \quad (11)$$

a_{13}= 1.0, a_{23} = 0.75, a_{33} = 0.17

Substituting the values of the constants, we have [*A*] matrix.

$$[A] = \begin{bmatrix}1 & 1 & 1\\0.25 & 0.55 & 0.75\\0.15 & 0.16 & 0.17\end{bmatrix} \quad (12)$$

This derived first three points are located on the vertices of the simplex factor space, however, the remaining three experimental points which are the interraction points are calculated by substituting in *Eq. 8* as follows;

For A_{12}

$$\begin{bmatrix}Z_1\\Z_2\\Z_3\end{bmatrix} = \begin{bmatrix}1 & 1 & 1\\0.25 & 0.55 & 0.75\\0.15 & 0.16 & 0.17\end{bmatrix} * \begin{bmatrix}0.5\\0.5\\0\end{bmatrix} = \begin{bmatrix}1\\0.4\\0.155\end{bmatrix} \quad (13)$$

For A_{13}

$$\begin{bmatrix}Z_1\\Z_2\\Z_3\end{bmatrix} = \begin{bmatrix}1 & 1 & 1\\0.25 & 0.55 & 0.75\\0.15 & 0.16 & 0.17\end{bmatrix} * \begin{bmatrix}0.5\\0\\0.5\end{bmatrix} = \begin{bmatrix}1\\0.5\\0.16\end{bmatrix} \quad (14)$$

For A_{23}

$$\begin{bmatrix}Z_1\\Z_2\\Z_3\end{bmatrix} = \begin{bmatrix}1 & 1 & 1\\0.25 & 0.55 & 0.75\\0.15 & 0.16 & 0.17\end{bmatrix} * \begin{bmatrix}0\\0.5\\0.5\end{bmatrix} = \begin{bmatrix}1\\0.65\\0.165\end{bmatrix} \quad (15)$$

The computation matrix table for the mixture proportion formulation is presented in *Table 1*.

Actual				Pseudo		
Z_1	Z_2	Z_3	Response	X_1	X_2	X_3
1	0.25	0.15	Y_1	1	0	0
1	0.55	0.16	Y_2	0	1	0
1	0.75	0.17	Y_3	0	0	1
1	0.4	0.155	Y_{12}	0.5	0.5	0
1	0.5	0.16	Y_{13}	0.5	0	0.5
1	0.65	0.165	Y_{23}	0	0.5	0.5

Table 1 Second order mixture formulation matrix table
1. táblázat Másodrendű keverék-összetétel mátrix táblázat

The experimental control points' mixture formulations are also calculated which were designed for the validation of the generated Scheffe's regression model.

For C_1

$$\begin{bmatrix}Z_1\\Z_2\\Z_3\end{bmatrix} = \begin{bmatrix}1 & 1 & 1\\0.25 & 0.55 & 0.75\\0.15 & 0.16 & 0.17\end{bmatrix} * \begin{bmatrix}0\\0.3333\\0.6667\end{bmatrix} = \begin{bmatrix}1\\0.683\\0.1667\end{bmatrix} \quad (16)$$

For C_2

$$\begin{bmatrix}Z_1\\Z_2\\Z_3\end{bmatrix} = \begin{bmatrix}1 & 1 & 1\\0.25 & 0.55 & 0.75\\0.15 & 0.16 & 0.17\end{bmatrix} * \begin{bmatrix}0.25\\0.65\\0.1\end{bmatrix} = \begin{bmatrix}1\\0.495\\0.1585\end{bmatrix} \quad (17)$$

For C_3

$$\begin{bmatrix}Z_1\\Z_2\\Z_3\end{bmatrix} = \begin{bmatrix}1 & 1 & 1\\0.25 & 0.55 & 0.75\\0.15 & 0.16 & 0.17\end{bmatrix} * \begin{bmatrix}0.1\\0.3\\0.6\end{bmatrix} = \begin{bmatrix}1\\0.64\\0.165\end{bmatrix} \quad (18)$$

For C_{12}

$$\begin{bmatrix}Z_1\\Z_2\\Z_3\end{bmatrix} = \begin{bmatrix}1 & 1 & 1\\0.25 & 0.55 & 0.75\\0.15 & 0.16 & 0.17\end{bmatrix} * \begin{bmatrix}0.6\\0.1\\0.3\end{bmatrix} = \begin{bmatrix}1\\0.43\\0.157\end{bmatrix} \quad (19)$$

For C_{13}

$$\begin{bmatrix}Z_1\\Z_2\\Z_3\end{bmatrix} = \begin{bmatrix}1 & 1 & 1\\0.25 & 0.55 & 0.75\\0.15 & 0.16 & 0.17\end{bmatrix} * \begin{bmatrix}0.1\\0.6\\0.3\end{bmatrix} = \begin{bmatrix}1\\0.58\\0.162\end{bmatrix} \quad (20)$$

For C_{23}

$$\begin{bmatrix}Z_1\\Z_2\\Z_3\end{bmatrix} = \begin{bmatrix}1 & 1 & 1\\0.25 & 0.55 & 0.75\\0.15 & 0.16 & 0.17\end{bmatrix} * \begin{bmatrix}0.65\\0.25\\0.1\end{bmatrix} = \begin{bmatrix}1\\0.375\\0.1545\end{bmatrix} \quad (21)$$

The computation matrix table for the mixture proportion formulation is presented in *Table 2*.

	Actual				Pseudo		
Runs	Z_1	Z_2	Z_3	Response	X_1	X_2	X_3
1	1	0.683	0.166	C_1	0	0.333	0.667
2	1	0.495	0.158	C_2	0.25	0.65	0.10
3	1	0.640	0.165	C_3	0.1	0.30	0.60
4	1	0.430	0.157	C_{12}	0.6	0.10	0.30
5	1	0.580	0.162	C_{13}	0.1	0.60	0.30
6	1	0.375	0.154	C_{23}	0.65	0.25	0.10

Table 2 Design matrix table for control points based on Scheffe's (3, 2) - lattice polynomial
2. táblázat Tervezési mátrix táblázat a vezérlőpontokhoz Scheffe (3, 2) - rácspolinom alapján

2.2 Responses

A simplex design expression will enable us to predict responses for different mixtures. Responses can be defined as a blend of selected properties of the additives or treatment matrix. For the soil-additive blend mixture, the constituent elements are water, kaolin, and soil. This approach is based on response surface methodology (RSM).

Hence, a simplex design expression will have the form [7, 29].

$$Y = b_0 + b_1x_1 + b_2x_2 + b_3x_3 + b_{11}x_1^2 + b_{12}x_1x_2 + b_{13}x_1x_3 + b_{22}x_2^2 + b_{23}x_2x_3 + b_{33}x_3^2 \quad (22)$$

Since the sum of the respective component for a ternary mixture as considered in this work

$$x_1 + x_2 + x_3 = 1 \;\; ie. \sum x_i - 1 = 0 \quad (23)$$

Where b is the constant coefficients, x_i the component proportions and Y is the response.

The reduced second-degree polynomial can be obtained as follows.

$$b_0x_1 + b_0x_2 + b_0x_3 = b_0 \quad (24)$$

$$b_0 = b_0(x_1 + x_2 + x_3) \quad (25)$$

Multiplying *Eq. 23* by x_1, x_2, x_3 in successions

$$x_1^2 = x_1 - x_1x_2 - x_1x_3 \quad (26)$$

$$x_2^2 = x_2 - x_1x_2 - x_2x_3 \quad (27)$$

$$x_3^2 = x_3 - x_1x_2 - x_2x_3 \quad (28)$$

Substituting *Eq. 24* into *Eq. 26, 27, 28*, we obtain after necessary transformation that.

$$\hat{Y} = (b_0 + b_1 + b_{11})x_1 + (b_0 + b_2 + b_{22})x_2 + (b_0 + b_3 + b_{33})x_3 + (b_{12} + b_{11} + b_{22})x_1x_2 + (b_{13} + b_{11} + b_{33})x_1x_3 + (b_{23} + b_{22} + b_{33})x_2x_3 \quad (29)$$

Simplifying as follows:

$$b_{ii} + b_i + b_0 = \beta \quad (30)$$

$$b_{ij} + b_{ii} + b_{jj} = \beta_{ij} \quad (31)$$

Eq. 29 becomes:

$$\hat{Y} = \beta_1x_1 + \beta_2x_2 + \beta_3x_3 + \beta_{12}x_1x_2 + \beta_{13}x_1x_3 + \beta_{23}x_2x_3 \quad (32)$$

Eq. 32 becomes the reduced second-degree polynomial.

Where:

$$Y_1 = \beta_1 \quad (33)$$

$$Y_2 = \beta_2 \quad (34)$$

$$Y_3 = \beta_3 \quad (35)$$

$$\beta_{12} = 4Y_{12} - 2Y_1 - 2Y_2 \quad (36)$$

$$\beta_{13} = 4Y_{13} - 2Y_1 - 2Y_3 \quad (37)$$

$$\beta_{23} = 4Y_{23} - 2Y_2 - 2Y_3 \quad (38)$$

3. Test materials

A kaolin sample was obtained from Agbaghara-Nsu in the Ehime Mbano Local Government Area of Imo State, Nigeria, using geological bedrock maps provided by the Geological Survey Agency of Nigeria for locating mineral deposits throughout the federation. The sample was crushed to a fine powder with an electric grinder (Model: 4E Grinding Mill, made in Germany) set to a gap width of 0.2 mm at 89 rpm. The crushed sample was sieved using a BS sieve set to obtain the desired powder form for easy mixing with the other mix constituents.

The soil sample was collected from a construction site at Alex Ekwueme Federal University Ndufu-Alike, Ikwo, Ebonyi State, Nigeria at a depth of 1.5 m using the disturbed sample technique. About 500 g of the sample was collected and the moisture content of the soil was determined before it was air dried for 7 days.

3.1 Methods

The experimental programs for the investigational study were carried out in accordance with the British Standard BS 1377-2 [30] for soil testing in civil engineering which is a widely recognized and accepted guideline. Following these guidelines ensures that the experimental programs are carried out with precision and accuracy, resulting in reliable results for Specific gravity testing, Atterberg limits, sieve analysis, and the California Bearing Ratio (CBR) test. The Kaolin, sample soil, and water sourced from a borehole within the laboratory are the three component materials in this mixture experiment problem [28].

3.1.1 California Bearing Ratio (CBR)

The California Bearing Ratio (CBR) is a standardized British test used to evaluate the strength and bearing capacity of subgrade and base course materials for roads, pavements, and other infrastructure projects. The test measures the ratio of the bearing capacity of a soil sample (in this case, a series of different variations of constituent components alongside sample soil mixes developed by the Scheffe mix design) to that of a standard crushed rock material. The test involves compacting the sample in a 2360 cm^3 mold using a 2.5 kg rammer in three layers. The first layer is compacted by dropping the rammer 25 times from a height of 30 cm. The second and third layers are compacted by dropping the rammer 50 times from a height of 15 cm. After compaction, the soil sample is allowed to be cured for 24 hours before the CBR test is conducted [31].

3.1.2 Specific gravity test

Based on the outline as described in BS 1377 [30] Part 4, the relative density of soil particles is gauged by the specific gravity of the soil. It is described as the proportion between the weight of an equal volume of soil particles and water. It can be used to determine the density, void ratio, and water content of soil. The specific gravity of soil is a crucial property for engineers and geotechnical experts. There are several ways to calculate soil's specific gravity, but the pycnometer method was used in this research study.

3.1.3 Compaction Test

The typical Proctor Test, also known as the compaction test, entails a lab procedure used to identify the ideal water for a specific compaction energy for a specific soil compaction energy. The purpose of this test is to determine whether soil has been compacted to the required density for use as a foundation for buildings, roads, and other structures. Although the Proctor Test is frequently used, there are other ways to assess the compaction properties of soil that might be more suitable for definite applications. For instance, the Scheffe mix design method entails developing unique soil mixtures using various constituent components and analyzing their laboratory compaction characteristics. This strategy can lead to more effective engineering by allowing them to adjust soil properties to specific project requirements [32].

4. Result and discussion

4.1 Characterization of test materials

The grain size distribution of the test soil from the laboratory experiments is represented as plotted in *Fig. 3*. From the obtained sieve analysis results, 80.5–6.15% are passing through sieve sizes of 2 mm–75 m, respectively. Tracing through the semi-log plot, the coefficients of gradation are derived as shown in *Eq. 39–41*. The obtained results indicate poorly graded silty clayey soil particles [33].

4.1.1 Test soil

$$C_u = \frac{D_{60}}{D_{10}} \quad (39)$$

$$C_c = \frac{D_{30}{}^2}{D_{60} \times D_{10}} \quad (40)$$

Coefficient of curvature $C_c = \frac{0.35^2}{0.75 \times 0.2} = 0.82$; Coefficient of Uniformity $C_u = \frac{0.75}{0.2} = 3.75$ (41)

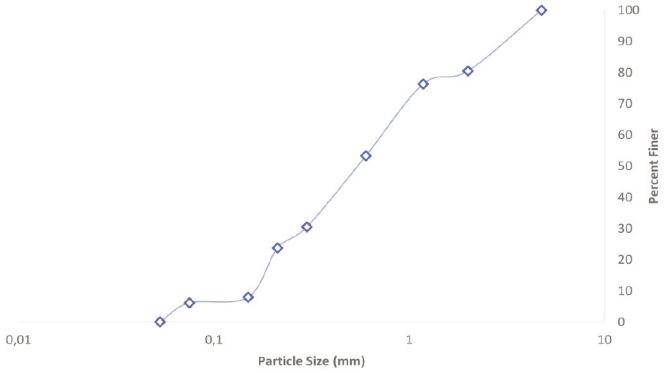

Fig. 3 Sieve analysis graph of the test soil
3. ábra A vizsgált talaj szitaelemzési grafikonja

The obtained laboratory results further showed that the soil has a specific gravity of 2.21 and a plasticity index of 17.67, which explains the plastic behavior of the sample soil. The AASHTO/USCS [34, 35] classification is A-7-6/CL, which indicates poorly graded silty clay soil with loose sedimentary materials and tiny rock particles. Applying the Atterberg limits in Casagrande's plasticity chart, the clay mineral identified is an inorganic clay of low plasticity. This soil type is rated poor for foundation and pavement construction purposes; hence, the need for stabilization. Also, the California bearing ratio test carried out on the soil sample showed a bearing capacity of 5.5%. These soil properties indicate inadequate conformance to the specifications of the Federal Ministry of Works for construction foundation materials [36, 37].

S/N	Properties	Standards	Result
1	Soil color	-	Reddish brown
2	Natural moisture content	BS 1377-2	23.4%
3	Specific gravity	BS 1377-2	2.21
4	% Passing sieve 0.075mm	BS 1377-2	6.15
5	Liquid limit	BS 1377-2	45.66
6	Plastic limit	BS 1377-2	27.99
7	Plasticity index	BS 1377-2	17.67
8	AASHTO /USCS classification	AASHTO 1986/ ASTM D 2487–11	A-7-6/CL
9	C.B. R	BS 1377-2	5.5%

Table 3 Properties of Sample soil
3. táblázat A talajminta tulajdonságai

The test for compaction showed the relationship between dry density and moisture content for different responses as shown in *Fig. 4* and *5* below.

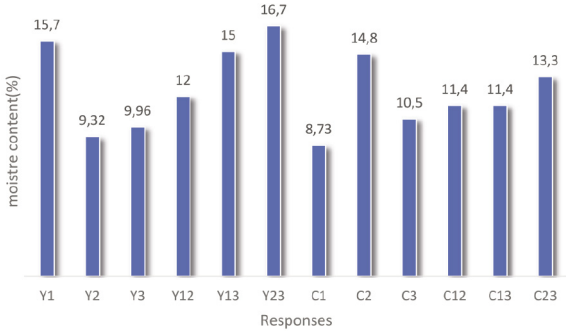

Fig. 4 Variations of Average Moisture Content
4. ábra Az átlagos nedvességtartalom változása

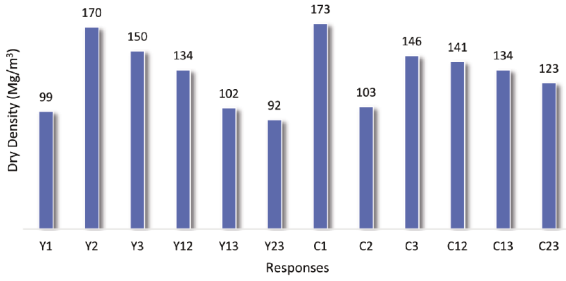

Fig. 5 Variations of Dry Density
5. ábra A száraz sűrűség változása

The derived laboratory results in comparison with the control experiment indicate a maximum average moisture content of 16.7% at experimental run Y_{23} and a minimum average moisture content of 9.32% at experimental point Y_2. Also, the dry density results obtained showed a maximum value of 170 mg/m³ at experimental point Y_2, and 92 mg/m³ at experimental run Y_{23} was recorded as the minimum value. Compaction property behavior can be said to show significant improvement at mix design experiment Y_{23}, which contains 35.81% kaolin, 9.09% water, and 55.10% test soil [38].

3.2 California Bearing Ratio (CBR)

The responses of the experimental, modelling and coefficients on the CBR exercise of the kaolin treated lateritic soil is represented in *Table 4* below.

Code	Z_1	Z_2	Z_3	Experimental response	X_1	X_2	X_3
Y_1	1	0.25	0.15	38.9	1	0	0
Y_2	1	0.55	0.16	76.6	0	1	0
Y_3	1	0.75	0.17	26.8	0	0	1
Y_{12}	1	0.4	0.155	59.1	0.5	0.5	0
Y_{13}	1	0.5	0.16	71.3	0.5	0	0.5
Y_{23}	1	0.65	0.165	68.1	0	0.5	0.5
C_1	1	0.68	0.166	58.7	0	0.333	0.667
C_2	1	0.50	0.159	70.0	0.25	0.65	0.1
C_3	1	0.64	0.165	68.4	0.1	0.3	0.6
C_{12}	1	0.43	0.157	71.3	0.6	0.1	0.3
C_{13}	1	0.58	0.162	75.5	0.1	0.6	0.3
C_{23}	1	0.38	0.154	60.6	0.65	0.25	0.1

Table 4 California bearing ratio responses from the experimental exercise and the model
4. táblázat Kaliforniai teherbírási arány a kísérletek és a modell alapján

The minimum condition for the use of a material as a Sub-base for pavement construction purposes in terms of CBR as stipulated by the Nigerian general specification for roads and bridges works volume III [39] to be 30% for sub-base. Based on the standard as stated, the peak value at 76.6% at mix design Y_2 for the unsoaked sample was recorded at a mix ratio of (1.00:0.55:0.16) for the sample soil, kaolin, and water respectively and thereafter there was a decrease in strength. Considering regression equation for the California bearing ratio from equ.33, 34, 35, 36, 37 and 38, and the experimental responses of the actual components, where.

$Y_1 = \beta_1 = 38.9$
$Y_2 = \beta_2 = 76.6$
$Y_3 = \beta_3 = 26.8$

And further substituting into *Eq. 36*, *37* and *38* for the values of β_1, β_2, β_3 respectively, the coefficients of the Scheffe's second-degree polynomials were as shown in *Table 5*.

Model coefficients					
β_1	β_2	β_3	β_{12}	β_{13}	β_{23}
38.9	76.6	26.8	5.4	153.8	65.6

Table 5 Coefficients of the Scheffe's second-degree polynomials
5. táblázat A Scheffe-féle másodfokú polinomok együtthatói

Further substitution of the values as shown in *Table 6* into *Eq. 32*, the values for the model responses were derived thus,

$$Y_{CBR} = 38.9x_1 + 76.6x_2 + 26.8x_3 + 5.4x_1x_2 + 153.8x_1x_3 + 65.6x_2x_3 \quad (42)$$

3.3 Test of adequacy of Scheffe's model developed

Eq. 42 is the modelled mathematical relationship to aid in optimization of California Bearing Ratio of kaolin stabilized Ikwo lateritic soil. Using the developed regression model in *Eq. 42*, the predicted results were determined and compared with the experimental test results to evaluate the prediction performance using the statistical methods ANOVA and the student's t-test [40, 41]. The compared and computed results are presented in *Fig. 6* and *Table 6*.

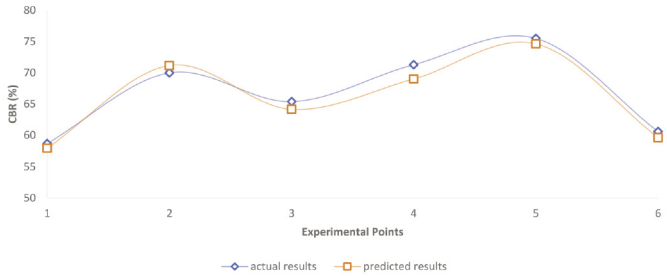

Fig. 6 Experimental and model predicted results
6. ábra A kísérleti és a modellel előre jelzett eredmények

s/n	Actual results	Predicted results
C_1	58.7	57.977
C_2	70.0	71.181
C_3	65.4	64.148
C_{12}	71.3	69.016
C_{13}	75.5	74.636
C_{23}	60.6	59.629

Table 6 Experimental and Scheffe's model predicted results
6. táblázat A kísérleti és a Scheffe-modell alkalmazásával előrejelzett eredmények

	Actual results	Predicted results
Mean	66.916	66.098
Variance	42.421	43.767
Observations	6	6
Pearson Correlation	0.985	
Df	5	
t Stat	1.776	
P(T<=t) one-tail	0.067	
t Critical one-tail	2.015	
P(T<=t) two-tail	0.135	
t Critical two-tail	2.570	

Table 7 Table t-Test statistical result
7. táblázat A t-teszt statisztikai eredménye

Scheffe's model is adequate for use in predicting the probable California bearing ratio strength properties of lateritic clayey soil-kaolin blend. The statistical model validation tests were carried out at 95% confidence interval using Microsoft Excel software. *P(T<=t)* two-tail of 0.1358 was obtained from the t-test and ANOVA respectively which indicates that the null hypothesis that there is no significant difference between the actual and Scheffe's models predicted values is accepted [42].

SUMMARY				
Groups	Count	Sum	Average	Variance
Actual results	6	401.5	66.916	42.421
Predicted results	6	396.6	66.098	43.767

Source of Variation	SS	Df	MS	F	P-value	F crit
Between Groups	2.010	1	2.010	0.046	0.833	4.964
Within Groups	430.944	10	43.094			
Total	432.954	11				

Table 8 Table ANOVA results
8. táblázat ANOVA eredmények

4. Conclusions

Based on the results, the reddish shelly Ikwo lateritic soil was classified as A-7-6 according to AASHTO and CL (inorganic clay) in the unified classification system of soil, respectively. The following conclusions were drawn:

1. The lateritic soil sample is a problematic soil with a low plasticity index.
2. The kaolin sourced from Agbaghara Nsu in its natural state can be a good pozzolana.
3. The kaolin sourced from Agbaghara Nsu can serve as a good binder for the stabilization of Ikwo lateritic soil.
4. A Scheffe second degree polynomial was successfully used in formulating a model for the prediction of the CBR behavior of the stabilized Ikwo lateritic soil.
5. The optimum mixture design was achieved.
6. The models developed from this thesis work provided a very good prediction of the responses used, and as such, this model

can be used in making critical decisions concerning the CBR of soil samples having similar geotechnical properties.

7. The student T-test and analysis of variance (ANOVA) test were used to check the validity of the models, and the model was found to be adequate at a 95% confidence level.
8. It was also concluded from the T-test and ANOVA statistical results that the P-value of 0.83 further explains that there is no significant difference between the actual CBR value, and the Scheffe model predicted value.

4.1 Recommendations

The requirement for a sub-base material can be said to be adequately satisfied by Ikwo lateritic soil when it's treated with Kaolin sourced from Agbaghara Nsu in Imo State. However, the behavior of this same sample soil will likely differ with the application of kaolin gotten from other sources.

However, the recommendation of its adequacy as a sub-base material is based on the prediction of the Scheffe mix design of **1:0.55:0.16** for the soil, kaolin, and water, respectively.

References

[1] Onyelowe, K. C. (2016). Kaolin stabilization of Olokoro lateritic soil using bone ash as admixture. International Journal of Constructive Research in Civil Engineering, 2(1). https://doi.org/10.20431/2454-8693.0201001

[2] Ikeagwuani, C. C., Nwonu, D. C. & Onah, H. N. Min-max fuzzy goal programming - Taguchi model for multiple additives optimization in expansive soil improvement. Int. J. Numer. Anal. Methods Geomech. https://doi.org/10.1002/nag.3163 (2020)

[3] Imoh Christopher Attah, George Uwadiegwu Alaneme, Roland Kufre Etim, Christopher Brownson Afangideh, Kufre Primus Okon & Obeten Nicholas Otu. Role of extreme vertex design approach on the mechanical and morphological behaviour of residual soil composite. Sci Rep (2023) 13:7933. https://doi.org/10.1038/s41598-023-35204-6

[4] Yaser Gamil, Kemas Ahmed Zamahri, Ismail Bakar (2018). Application of Scheffe's Theory to Develop Mathematical Prediction Model to Predict UCS for Hybrid Containing Organic Soil and POFA-OPC Additives. Civil Engineering and Architecture, 6(2), 54 - 64. https://doi.org/10.13189/cea.2018.060202

[5] Attah, I. C., Agunwamba, J. C., Etim, R. K. & Ogarekpe, N. M. Modelling and predicting of CBR values of lateritic soil treated with metakaolin for road material. ARPN J. Eng. Appl. Sci. 14(20), 3609–3618 (2019)

[6] Usoh, G. A., Ahaneku, I. E., Ugwu, E. C., Sam, E. O., Itam, D. H., Alaneme, G. U., & Ndamzi, T. C. (2023). Mathematical modeling and numerical simulation technique for selected heavy metal transport in MSW dumpsite. Scientific Reports, 13(1), 5674. https://doi.org/10.1038/s41598-023-32984-9

[7] H. Scheffé, Experiments with mixtures, J. R. Stat. Soc. B 20 (1958) 344–360.

[8] Imoh Christopher Attah, Roland Kufre Etim, George Uwadiegwu Alaneme, David Ufot Ekpo. (2022).Scheffe's approach for single additive optimization in selected soils amelioration studies for cleaner environment and sustainable subgrade materials. Cleaner Materials, 100126, ISSN 2772-3976, https://doi.org/10.1016/j.clema.2022.100126

[9] H. Scheffé, The simplex-centroid design for experiments with mixtures, J. R. Stat. Soc. B 25 (1963) 235–263.

[10] Kennedy Onyelowe, George Alaneme, Duc Bui Van, Manh Nguyen Van, Charles Ezugwu, Talal Amhadi, Felix Sosa, Francis Orji, Benjamin Ugorji, Generalized Review on EVD and Constraints Simplex Method of Materials Properties Optimization for Civil Engineering, Civil Engineering Journal (5) (2019) 729-749, http://dx.doi.org/10.28991/cej-2019-03091283

[11] Attah, I. C., Okafor, F. O. & Ugwu, O. O. Optimization of California bearing ratio of tropical black clay soil treated with cement kiln dust and metakaolin blend. Int. J. Pavement Res. Technol. 14(6), 655–667. https://doi.org/10.1007/s42947-020-0003-6 (2021)

[12] U. Alaneme George and M. Mbadike Elvis, (2019) optimization of flexural strength of palm nut fiber concrete using Scheffe's theory, Materials Science for Energy Technologies 2 (2019) 272–287.

[13] Ambrose, E. E., Okafor, F. O., & Onyia, M. E. (2021). Compressive strength and Scheffe's optimization of mechanical properties of recycled ceramics tile aggregate concrete. Epitoanyag - Journal of Silicate Based and Composite Materials, 73(3), 91-102. https://doi.org/10.14382/epitoanyag-jsbcm.2021.14

[14] Ogunsanwo, A. O., Afolabi, A. O., & Onwuka, O. O. (2016). Application of Scheffe optimization models on soil stabilization. Construction and Building Materials, 113, 104-111.

[15] Ogunsanwo, A. O., Afolabi, A. O., & Onwuka, O. O. (2019). Scheffe Optimization Models for Soil Stabilization: A Review. International Journal of Scientific & Engineering Research, 10(4), 1-7.

[16] Oguaghamba, E. C., & Okafor, I. C. (2021). Application of Scheffe's Model for stabilization of Amuro-okigwe subgrade using male inflorescence of oil palm ash. Nigerian Journal of Technology, 40(1), 1-10. https://doi.org/10.4314/njt. v40i1.10

[17] J. T. Ding, P. Y. Yan, S. L. Liu, and J. Q. Zhu, "Extreme vertices design of concrete with combined mineral admixtures," Cement and Concrete Research, vol. 29, no. 6, pp. 957–960, 1999

[18] Ewa, D.E., Ukpata, J.O., Otu, O.N. et al. Optimization of saw dust ash and quarry dust pervious concrete's compressive strength using Scheffe's simplex lattice method. Innov. Infrastruct. Solut. 8, 64 (2023). https://doi.org/10.1007/s41062-022-01031-3

[19] Ewa DE, Ukpata JO, Otu ON, Memon ZA, Alaneme GU, Milad A. Scheffe's Simplex Optimization of Flexural Strength of Quarry Dust and Sawdust Ash Pervious Concrete for Sustainable Pavement Construction. Materials. 2023; 16(2):598. https://doi.org/10.3390/ma16020598

[20] Okere, C. (2013). Simplex-based concrete mix design. IOSR Journal of Mechanical and Civil Engineering, 5(2), 46-55. https://doi.org/10.9790/1684-0524655

[21] Attah, I.C., Etim, R.K., Alaneme, G.U., Bassey O. B. (2020). Optimization of mechanical properties of rice husk ash concrete using Scheffe's theory. SN Appl. Sci. **2,** 928 (2020) https://doi.org/10.1007/s42452-020-2727-y

[22] Alaneme, G.U., Attah, I.C., Etim, R.K. and M. U. Dimonyeka (2021). Mechanical Properties Optimization of Soil—Cement Kiln Dust Mixture Using Extreme Vertex Design. Int. J. Pavement Res. Technol. https://doi.org/10.1007/s42947-021-00048-8

[23] Chiemela, C., Okoye, P. C., Nwosu, P. C., Oke, O. M., & Ohakwe, C. N. (2014). Optimization of concrete made with Abakaliki quarry dust as fine aggregate using Scheffe's optimization model. International Letters of Natural Sciences, 20, 115-128. https://doi.org/10.18052/www.scipress.com/ilns.20.115

[24] Alaneme, G., Mbadike, E (2020). Modelling of the compressive strength of palm-nut-fibre concrete using scheffe's theory. Computational Engineering and Physical Modeling, 3(1), 31-40. https://doi.org/10.22115/cepm.2020.212999.1076

[25] Alaneme, G.U., Iro, U.I., Milad, A. et al. Mechanical Properties Optimization and Simulation of Soil–Saw Dust Ash Blend Using Extreme Vertex Design (EVD) Method. Int. J. Pavement Res. Technol. (2023). https://doi.org/10.1007/s42947-023-00272-4

[26] Ikeagwuani, C. C., Agunwamba, J. C., Nwankwo, C. M. & Eneh, M. Additives optimization for expansive soil subgrade modifcation based on Taguchi grey relational analysis. Int. J. Pavement Res. Technol. https://doi.org/10.1007/s42947-020-1119-4 (2020)

[27] Alaneme George Uwadiegwu & Mbadike Elvis Michael. (2021). Characterization of Bambara Nut Shell Ash (BNSA) in Concrete Production. Jurnal Kejuruteraan 33(3) 2021: 621-634. https://doi.org/10.17576/jkukm-2021-33(3)-21

[28] Aju, D.E., Onyelowe, K.C., Alaneme, G.U., Constrained vertex optimization and simulation of the unconfined compressive strength of geotextile reinforced soil for flexible pavement foundation construction, Cleaner Engineering and Technology (2021) https://doi.org/10.1016/ j.clet.2021.100287

[29] A. Ozol-Godfrey, C. M. Anderson-Cook, and D. C. Montgomery, "Fraction of design space plots for examining model robustness," Journal of Quality Technology, vol. 37, no. 3, pp. 223–235, 2005

[30] BS 1377. (2022). Methods of test for soils for civil engineering purposes. General requirements and sample preparation.

[31] Attah, I.C., Agunwamba, J.C., Etim, R.K., Ogarekpe, N.M., 2019. Modelling and predicting of CBR values of lateritic soil treated with metakaolin for road material. ARPN J. Eng. Appl. Sci. 14 (20), 3609–3618.

[32] Gregory C. Ezeokpube, Isiguzo Edwin Ahaneku, George Uwadiegwu Alaneme, Imoh Christopher Attah, Roland Kufre Etim, Bamidele Charles Olaiya, and Iberedem Monday Udousoro (2022). Assessment of Mechanical Properties of Soil-Lime-Crude Oil-Contaminated Soil Blend Using Regression Model for Sustainable Pavement Foundation Construction. Advances in Materials Science and Engineering Volume 2022, Article ID 7207842, 18 pages https://doi.org/10.1155/2022/7207842

[33] Jalal, F. E., Xu, Y. & Jamhiri, B. Memon SA (2020). On the recent trends in expansive soil stabilization using calcium-based stabilizer materials (CSMs): A comprehensive review. Adv. Mater. Sci. Eng. https://doi.org/10.1155/2020/1510969 (2020)
[34] Onyelowe KC, Alaneme GU, Onyia ME, Bui Van D, Diomonyeka MU, Nnadi E, Ogbonna C, Odum LO, Aju DE, Abel C, Udousoro IM, Onukwugha E (2021) Comparative modeling of strength properties of hydrated-lime activated rice-husk-ash (HARHA) modified soft soil for pavement construction purposes by artificial neural network (ANN) and fuzzy logic (FL). Jurnal Kejuruteraan 33(2) 2021: 365-384 https://doi.org/10.17576/jkukm-2021-33(2)-20
[35] AASHTO (1986): "Standard Specifications for Transportation, Material and Method
[36] USCS (Unified Soil Classification System). (1998). Unified Soil Classification System. American Society for Testing and Materials (ASTM), West Conshohocken, PA, USA
[37] Alaneme, G.U., Dimonyeka, M.U., Ezeokpube, G.C. et al. Failure assessment of dysfunctional flexible pavement drainage facility using fuzzy analytical hierarchical process. Innov. Infrastruct. Solut. 6, 122 (2021). https://doi.org/10.1007/s41062-021-00487-z
[38] Alaneme, G. U., Onyelowe, K. C., Onyia, M. E., Bui Van, D., Mbadike, E. M., Ezugwu, C.N., Dimonyeka, M. U., Attah, I. C., Ogbonna, C., Abel, C., Ikpa, C. C., and Udousoro I. M. (2020). Modeling Volume Change Properties of Hydrated-Lime Activated Rice Husk Ash (HARHA) Modified Soft Soil for Construction Purposes by Artificial Neural Network (ANN), Umudike Journal of Engineering and Technology, Vol. 6 (1), pp. 88 -110. https://doi.org/10.33922/j.ujet_v6i1_9
[39] Nigerian General Specification (1997): "Bridges and Roadworks" Vol.11, Federal Ministry of Works, Lagos
[40] Ezeh, J. C., & Ibearugbulem, O. M. (2009). Application of Scheffe's Model in Optimization of Compressive cube Strength of River Stone Aggregate Concrete. International Journal of Natural and Applied Sciences, 5(4)
[41] Ujong, J.A., Mbadike, E.M. & Alaneme, G.U. Prediction of cost and duration of building construction using artificial neural network. Asian J Civ Eng (2022). https://doi.org/10.1007/s42107-022-00474-4
[42] Uzoma Ibe Iro, George Uwadiegwu Alaneme, Abdalrhman Milad, Bamidele Charles Olaiya, Obeten Nicholas Otu, Edward Uchenna Isu, and Magnus Nnaemeka Amuzie. (2022). Optimization and Simulation of Saw Dust Ash Concrete Using Extreme Vertex Design Method. Advances in Materials Science and Engineering Volume 2022, Article ID 5082139, 22 pages https://doi.org/10.1155/2022/5082139

Ref.:
Ikpa, Chidozie Chimereze – **Ike**, Charles Chinwuba – **Alaneme**, George Uwadiegwu: *Scheffe optimization of the California Bearing Ratio of a kaolin blended lateritic soil for pavement construction*
Építőanyag – Journal of Silicate Based and Composite Materials, Vol. 75, No. 2 (2023), 58–66. p.
https://doi.org/10.14382/epitoanyag-jsbcm.2023.09

The effect of temperature rise on the thermal conductivity of composite (perovskite/polymer) solar cell

Tawfeeq W. MOHAMMED ▪ Materials Engineering Dept., Mustansiriyah University, Iraq ▪ tawfeeqwasmi@uomustansiriyah.edu.iq

Moafaq K.S. AL-GHEZI ▪ Mechanical Engineering Dept., University of Technology, Iraq ▪ moafaq.k.shiea@uotechnology.edu.iq

Ibrahim A. ATEA ▪ Materials Engineering Dept., Mustansiriyah University, Iraq ▪ ibrahim1980@uomustansiriyah.edu.iq

Érkezett: 2022. 10. 31. ▪ Received: 31. 10. 2022. ▪ https://doi.org/10.14382/epitoanyag-jsbcm.2023.10

Abstract

The efficiency of solar cell and the corresponding output power is mainly affected by the rise in the film temperature, and in such cases, the stability in thermal conductivity value is required to ensure adequate rate of heat loss. This study investigates the effect of temperature rise on the overall thermal conductivity of the perovskite cell including the response of polymeric additives that have been used recently to enhance the interaction between different grains in perovskite films. The polymers under study are: polyethylene oxide (PEO), polyacetylene (PA), polythiophene (PT), polystyrene (PS) and polymethyl methacrylate (PMMA). The work assumes mathematical procedure that links the variation of temperature to the degree of polymer's crystallinity and then converting this impact in terms of thermal conductivity. The calculations assumed three different concentrations of the polymer as: 1, 3 and 5%. Each polymer has served with two degrees of crystallinity. In general, the results show that the effect of added polymers on the final value of the thermal conductivity of the film may be positive or negative depending on three main factors: k-value of the perovskite-based material, k-value of the polymer and concentration of the polymer. The effect of the polymer appears more when it is used with the low k-value perovskite material (0.2 W/m·K) rather than with high k-value perovskite material (0.8 W/m·K). The addition of PEO to the perovskite-based materials makes the overall k-value of the film reaches to 3.7 W/m·K and even higher when the temperature rises up. Hence, this polymer is useful in high operation temperature. In the case of using polymers (PA and PT), the overall k-value of the film was less sensitive. The use of amorphous polymers (PS and PMMA) has not witnessed any significant contribution in the overall k-value of the film.

Keywords: temperature rise, thermal conductivity, polymers, perovskite, solar cells
Kulcsszavak: hőmérséklet-emelkedés, hővezető képesség, polimerek, perovszkit, napelemek

Tawfeeq W. MOHAMMED
is a university teacher in Mustansiriyah University, Iraq. He has a PhD in Mechanical Engineering. He teaches Heat Transfer and Thermodynamics, and has many researches in renewable energies and energy conservation.

Moafaq K.S. AL-GHEZI
is a university teacher in University of Technology, Iraq. He has a PhD in Mechanical Engineering. He is the head of Solar Energy Research Center, and has many researches in renewable energies.

Ibrahim A. ATEA
is a university teacher in Mustansiriyah University, Iraq. He has a MSc in Materials Engineering. He teaches Semiconductor Materials, and has many researches in this field.

1. Introduction

Recently, solar cells including many categories, such as: silicone-based cells, concentrated photovoltaics, organic photovoltaics, cadmium telluride cells, copper indium gallium selenide (CIGS) cells, multi-junction cells, tandem cells, quantum-dot cells and perovskite cells. These types have been receiving attention from both researchers and manufacturers [1]. A perovskite solar cell is a developed type of solar cells which includes perovskite-structured compounds, mostly semiconductors such as: calcium titanium oxides with hybrid organic-inorganic lead-based materials or tin halide-based materials. The materials used in the perovskite type have witnessed many improvements to become more economic as well as energy efficient, where maximum efficiency has reached up to 25% [2-6]. The characteristics of organic-inorganic perovskite regions are the interest for recent studies to develop the performance of these cells by enhancing many preferable parameters such as: absorption coefficient, bandgap, carrier mobility and carrier lifetime [7, 8]. The crystallization of the cells is another imperative feature for high performance perovskite cells, where it is related to the light absorption and carrier transportation. The presence of defects and crosslinking patterns may affect the performance of the cells by accelerating the carriers' recombination. Therefore, more attention has been seeking to reduce the defects and pinholes in order to obtain perfect perovskite cells [9-11].

Polymeric materials have been involved in perovskite cells as additives to enhance the general performance of the solar film and the overall conversion efficiency. In this aspect, common polymers that are used include: polyethylene oxide (PEO), polyvinylpyrrolidone (PVP), polyacrylonitrile (PAN), polyetherimide (PEI), polymethyl methacrylate (PMMA), polyacetylene (PA), polythiophene (PT), polystyrene (PS) and some other polymers [12-15]. From previous studies, polymers can be used as additives to improve the crystallization morphology by enhancing the interaction between different grains in perovskite films [16, 17], and by facilitating the nucleation and regulating the crystal growth [18-20]. Polymers can be immersing easily in polar solvents, which reduces the contact angle [21] and increases the device stability [22, 23]. Furthermore, polymers demonstrated for the improving of electrical, optical and other physical properties of perovskite-structured materials [24-31].

Polymers usually have med-to-high degree of crystallinity, where the structure of the molecules is identical partially. The degree of crystallinity has a big influence on many thermo-physical properties as well as mechanical features. However, synthetic polymers are usually semi-crystalline and their degrees of crystallinity are typically range between 10-80% [32-35]. The degree of crystallinity is an important factor affecting the thermal conductivity of semi-crystalline polymers. Where, maximum thermal conductivity achieved at high degree of crystallinity, where packed structure accelerate the heat [34]. However, in semi-crystalline polymers, thermal conductivity above room temperature gradually decreases by the increasing of temperature. This can be attributed to the loss of crystalline regions due to the heat flow [36-39]. Since, the most of solar radiation incident on the film is not converted into electricity, but it is absorbed as a heat thus it rises up the film temperature which causes a reduction in the efficiency. Access heat can be removed from internal layers mainly by heat conduction, which is related to the thermal conductivity of the material. Therefore, higher heat conductivity means efficient performance, and thus higher output power [40-45]. Hence, when temperature rises, a variation in thermal conductivity of the polymer affects the cell performance.

The object of the current study is to predict theoretically the effective thermal conductivity of the perovskite film due to the thermal behavior of polymeric additives that influence the overall performance of the solar cell. It is worth to mention that there is limited literature regarding the thermal conductivity of composite perovskite/polymer films. The novelty of the study is to present a mathematical model that links the effect of temperature on thermal conductivity of polymeric additives (with their specific concentration ratio and degree of crystallinity) to the overall thermal conductivity of the perovskite solar cell.

2. Materials and methods

In order to find the variation in the thermal conductivity of perovskite film including the thermal behavior of polymeric additives in the cell, some common polymeric materials are considered, such as: polyethylene oxide (PEO), polyacetylene (PA), polythiophene (PT), polystyrene (PS) and polymethyl methacrylate (PMMA). These materials show different features and wide range of thermo-physical properties, as shown in *Table 1*.

Polymer	Degree of crystallinity (%)	Density of crystalline structure (g/cm³)	Density of amorphous structure (g/cm³)	Thermal conductivity of crystalline structure (W/m·K)
PEO	60-80 [46]	1.24 [47]	1.12 [47]	60 [48]
PA	50-70 [49]	0.6 [50]	0.4 [50]	0.95 [51]
PT	40-60 [52]	1.18 [53]	1.12 [53]	0.62 [51]
PS	3-8 [54]	1.05 [55]	1.03 [55]	0.18 [56]
PMMA	~ 0 [57]	1.19 [57]	1.19 [57]	0.16 [58]

Table 1. Thermo-physical properties of polymers (pure solid additives)
1. táblázat A polimerek hőfizikai tulajdonságai (tiszta szilárd adalékok)

Since the intended goal is to determine the change in thermal conductivity of these polymeric materials due to the variation in the temperature of the film, hence the current mathematical procedure suggests finding the variation in the temperature with respect to an intermediate parameter which is the degree of the crystallinity, and then seeking to link this parameter to the thermal conductivity of the polymer and corresponding impact on the thermal conductivity of solar cell as overall.

The thermal conductivity of common polymeric materials is usually ranged between 0.2-1.0 W/m·K, with unique values for some others [35]. Polymers with high thermal conductivity values are required when the purpose is to release the heat. Many factors affect the thermal conductivity of a material such as: temperature, density, porosity, moisture, degree of crystallinity, chain structure, orientation of grains, size of molecules and impurities [59, 60]. The coefficient of thermal conductivity of polymers has different behaviors whether the polymer is thermoplastic or thermosetting, crystalline or amorphous and below or above glass-transition temperature [61, 62]. The increasing of the crystallinity leads to increase the thermal conductivity, thus thermal conductivity of crystalline region is higher than thermal conductivity of amorphous region [63-65]. However, the thermal conductivity of a semi-crystalline polymer is given by [34]:

$$k_{po} = X_c\, k_c + (1\text{-}X_c)\, k_a \quad (1)$$

Where;
k_{po}: thermal conductivity of the semi-crystalline polymer.
k_c: thermal conductivity of crystalline part.
k_a: thermal conductivity of amorphous part.
X_c: degree of crystallinity of the polymer.

The last equation can be re-written as;

$$k_{po} = [(1 - Z)\, X_c + Z]\, k_c \quad (2)$$

Where (Z) is the ration between (k_a) and (k_c).

Since, the thermal conductivity is influenced by the density, where the higher density material has the higher thermal conductivity and the increasing in the crystallinity of the polymer leads to increase both: density and thermal conductivity in the same manner [66]. Thus, the ratio (Z) can be presented in terms of density, as following;

$$Z = \rho_a / \rho_c \quad (3)$$

During temperature rise, the thermal conductivity of the semi-crystalline polymers (PEO, PA and PT) decreases with respect to the increasing in the temperature. This can be attributed to the phenomenon of Umklapp scattering process, which occurs in the boundary of lattice where it increases the momentum of phonon. By rising the temperature, this process becomes more frequent and the phonon free path decreases, thus less ability to conduct the heat [61, 62]. For PS and PMMA, since the structure of these polymers is amorphous, so they show different behavior with temperature. Where, the thermal conductivity increases with the increasing of the temperatures in association with the increasing of the specific heat, and this attributed to the increase of the thermal activation of

the phonons due to the molecular vibration within the lattice [58, 61].

Hence, the general form of thermal conductivity-temperature relationship has the following linear formula:

$$k_p = k_{po} + \mu T \quad (4)$$

Where:
k_p: thermal conductivity of the polymer as a function of temperature.
k_{po}: thermal conductivity of the polymer at room temperature.
μ: index of variation.
T: temperature.

The index of the variation with the temperature within the range 20-100 °C can be extracted from specific studies that investigated the temperature effect on the thermal conductivity of the selected polymers, as shown in *Table 2*.

Polymer	Index of variation
PEO	- 0.3 [48]
PA	- 0.004 [51]
PT	- 0.002 [51]
PS	+ 0.0006 [56]
PMMA	+ 0.0008 [56, 58]

Table 2 The index of variation of thermal conductivity of polymers with the temperature
2. táblázat A polimerek hővezető képességének változási indexe a hőmérséklet függvényében

Perovskite-based materials usually have thermal conductivity values between 0.2-0.8 W/m·K at room temperature, and it may be even more for some compositions [67, 68]. During the operating and exposing to sunlight, high film temperature can lead to the degradation of perovskite solar cells due to burn-in, defects formation, films cracking, and delamination at the layers' interfaces. Keeping high thermal conductivity is essential to reduce the film temperature and facilitating the dissipation of accumulated heat. However, the interested thing about these materials is that as temperature increases, many parameters increases as well, such as: number of free electrons, lattice vibrations, thermal activation of the phonons and specific heat [69]. Thus, the thermal conductivity of the perovskite-based material is expected to increase. It is noticed that the variation of thermal conductivity with the temperature (within 20-100 °C) for low *k*-value of perovskite material is generally has the form [70, 71]:

$$k_v = k_{vo} + 0.001\ T \quad (5)$$

Where, k_{vo} is the *k*-value of the perovskite-based material at room temperature. While, the variation of *k*-value with the temperature for high thermal conductivity perovskite material is generally appeared as [72, 73]:

$$k_v = k_{vo} + 0.02\ T \quad (6)$$

Finally, the overall *k*-value of the whole perovskite film is the summation of both *k*-value of perovskite-based materials (k_v) and *k*-value of polymeric additives (k_p) according to the mixing rule of composite materials and depending on the content of perovskite-based materials (φ_v) and the content of polymeric materials (φ_p). Thus:

$$k = k_v\ \varphi_v + k_p\ \varphi_p \quad (7)$$

Take into account that the concentration of polymeric materials involved within the whole structure of the film in the perovskite cell is between 1-5 wt% [12-31].

3. Results and discussion

This study includes theoretical analysis to predict the overall thermal conductivity of the perovskite film including the variation happens in the thermal conductivity of polymers that usually involved within the film to enhance the performance of the solar cell. As mentioned previously, five types of polymeric materials have been included in the calculations with their properties. The polymers are: polyethylene oxide (PEO), polyacetylene (PA), polythiophene (PT), polystyrene (PS) and polymethyl methacrylate (PMMA). The calculations assumed three different concentrations of the polymeric additives as: 1, 3 and 5%. Each polymer has served with two degrees of crystallinity; i.e. the maximum value and the minimum value. The thermal conductivity of the perovskite-based material has two values as; 0.2 and 0.8 W/m·K (designed values). The range of temperatures considered was between 20-100 °C.

In general, the low thermal conductivity of perovskite composites is attributed to the shorter lifetimes of the optical phonons and the smaller group velocity of acoustic phonons [73]. Take into account the effects of the values and distribution of band gaps [74].

The results show that the effect of added polymers on the final value of the thermal conductivity of the film may be positive or negative depending on three main factors: *k*-value of the perovskite-based material, *k*-value of the polymer and concentration of the polymer. As for the degree of crystallinity, it had no significant effect because the variance in the *k*-value was very small. Also, the effect of the polymer appears more when it is used with the low *k*-value perovskite material (0.2 W/m·K) because of the closeness of this *k*-value with the *k*-value of the polymer. But when it is used with the high *k*-value perovskite material (0.8 W/m·K), the perovskite will dominate for two reasons; firstly, its high *k*-value compared to the polymer, and secondly because of the accelerated increase of this value when the temperature rises comparing to the slow change that occurring on the *k*-value of the polymer.

The deep analysis of the results has shown that the thermal conductivity of semi-crystalline polymers (PEO, PA and PT) has decreased by the increasing in the temperature, due to less mean free path of phonons, thus it may have a negative impact on the overall thermal conductivity of the perovskite film. On the other hand, the thermal conductivity of amorphous polymers (PS and PMMA) has increased by the increasing in the temperature, due to thermal activation of the phonons, thus it may have a positive impact on the thermal conductivity of overall perovskite cell. However, each polymer has shown some interesting behaviors and intervention effects of polymeric concentration and thermal conductivity of perovskite-based materials.

The addition of PEO to the film has introduced a unique contribution as a semi-crystalline polymer to the perovskite cell due to its high thermal conductivity value (60 W/m·K). This makes the overall *k*-value of the film reaches until (3.7 W/m·K) at room temperature which is higher than the *k*-value of the perovskite-based material and it remains high at any range of temperatures or polymeric concentrations, as shown in *Fig. 1*. The overall *k*-value was between 0.7-3.0 W/m·K for the film of perovskite-based thermal conductivity of (0.2 W/m·K), and between 1.3-4.0 W/m·K for the film of perovskite-based thermal conductivity of (0.8 W/m·K). Hence, this polymer can be useful in application requires efficient heat conduction and thus to obtain higher power efficiency. However, for low perovskite thermal conductivity (0.2 W/m·K), the rise in the temperature up to 100 °C has shown a decreasing in the *k*-value by 25-45% in comparing to the reference value at room temperature (20 °C). While, for high perovskite thermal conductivity (0.8 W/m·K), the rise in the temperature up to 100 °C has shown an increasing in the *k*-value by 10-90% in comparing to the reference value at room temperature. The decreasing in the first case is mainly due to the polymer thermal behavior which was the dominant, where at low value of perovskite *k*-value (0.2 W/m·K) and its corresponding thermal response which was low comparing to the highly response of the polymer that made the overall film follows the polymer behavior. While, in the second case (k_v=0.8 W/m·K), the thermal response of the perovskite was higher, thus the overall film follows the perovskite behavior not the polymer. Furthermore, the increasing in the degree of crystallinity of the polymer from 60 to 80% enhanced the thermal conductivity of the film by 2-3% only, which is disappointed. Note that the increasing in the PEO concentration results in even higher *k*-values in overall.

In the case of using polymers (PA and PT) that have relatively closest thermal conductivity values to the perovskite-based materials, the overall *k*-value of the film was less sensitive to the thermal behavior of the polymeric materials, especially at the high design *k*-value (0.8 W/m·K). The results of adding PA to the film, shown in *Fig. 2*, have revealed an effective thermal conductivity usually more than the designed value at any range of temperatures or polymeric concentrations. However, at low design *k*-value (0.2 W/m·K), the behavior of increasing in overall *k*-value is attributed to the fact that the *k*-value of the polymer was higher in comparing to the perovskite-based material, even though the decreasing ratio in the polymer *k*-value was higher than the increasing ratio in the perovskite *k*-value. At high design *k*-value (0.8 W/m·K), the sensitivity of polymer effect was relatively less due to higher *k*-value of the perovskite-based material compared to the polymer, and secondly because of the faster increase in the *k*-value of the perovskite-based material with the temperature comparing to the slow decreasing in the *k*-value of the polymer. A similar behavior can be seen by the adding of PT to the film, as shown in *Fig. 3*, with even less influence due to the lower *k*-value of PT than that of PA, and corresponding thermal response of PT which was lower than that of PA. However, the rise in the temperature up to 100 °C increased the referenced *k*-value of the film for both PA and PT up to 50% for (k_v=0.2 W/m·K) and up to 150% for (k_v=0.8 W/m·K), where this is actually the same increasing in the *k*-value of the perovskite-based materials. Also, the enhancement in *k*-value due to increasing in the degree of crystallinity of the polymer was negligible.

In case of adding amorphous polymers (PS and PMMA), that already have low values of thermal conductivity and slow thermal response, the overall *k*-value of the film is rather a function of perovskite-based materials only, even at high temperatures, as shown in *Fig. 4* and *5*, respectively. However, the involving of more than 1% of these polymers within the film was not sufficient to rise the effective thermal conductivity higher, thus it may be a useless choice in the design.

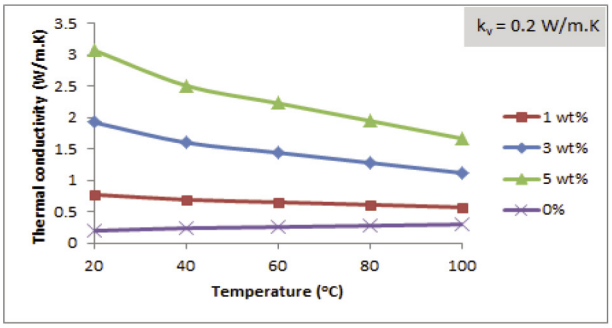

a. X_c=60% & k_v=0.2 W/m.K

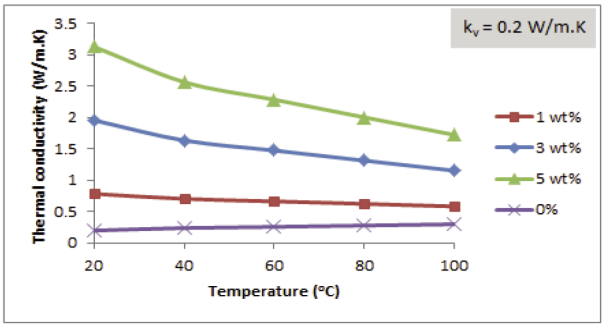

b. X_c=80% & k_v=0.2 W/m.K

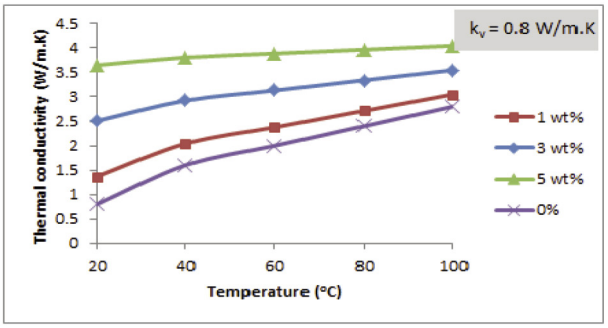

c. X_c=60% & k_v=0.8 W/m.K

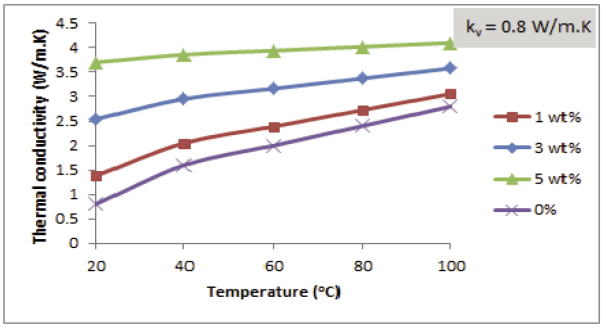

d. X_c=80% & k_v=0.8 W/m.K

Fig. 1 Overall thermal conductivity of perovskite cell at different PEO concentrations
1. ábra Perovszkit cella teljes hővezető képessége különböző PEO koncentrációk mellett

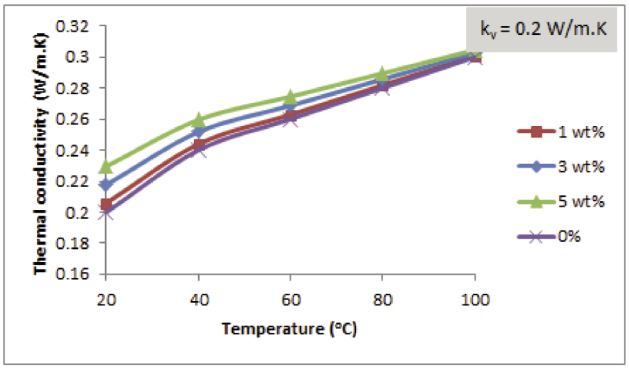

a. X_c=50% & k_v=0.2 W/m.K

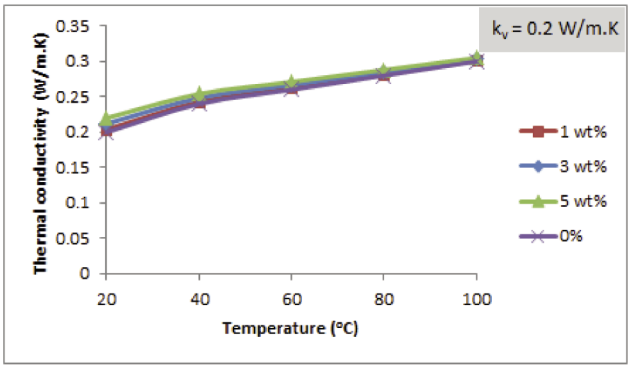

a. X_c=40% & k_v=0.2 W/m.K

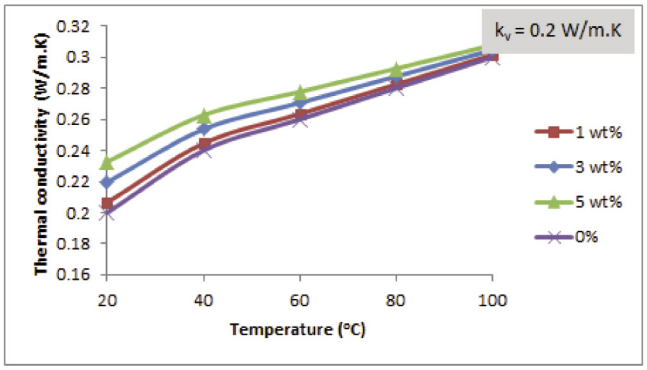

b. X_c=70% & k_v=0.2 W/m.K

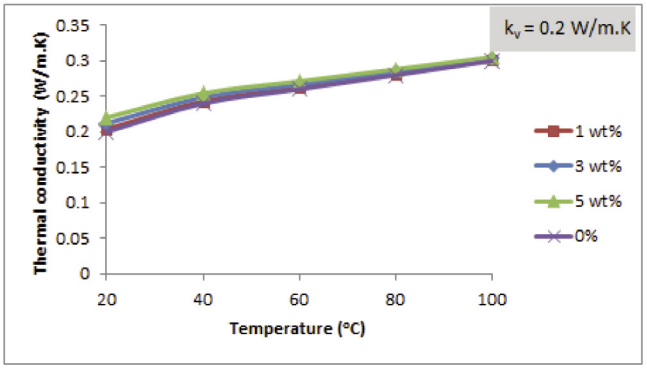

b. X_c=60% & k_v=0.2 W/m.K

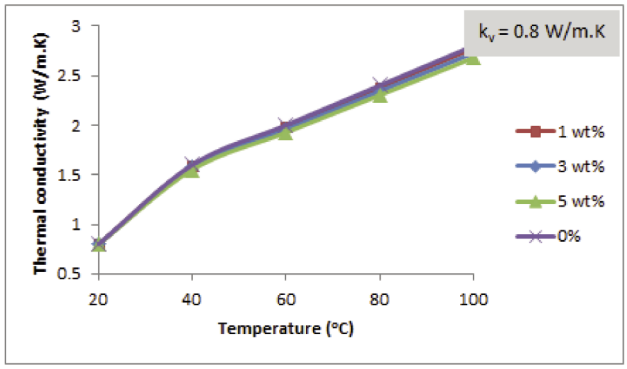

c. X_c=50% & k_v=0.8 W/m.K

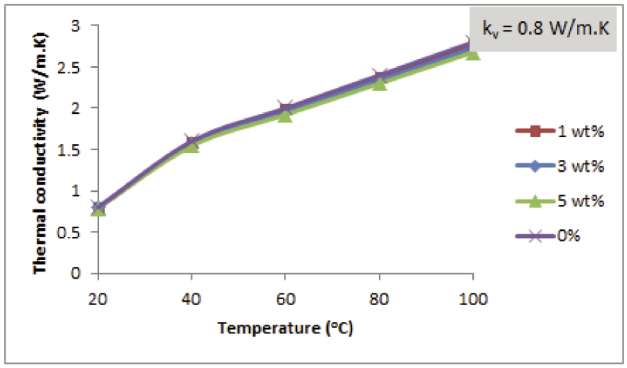

c. X_c=40% & k_v=0.8 W/m.K

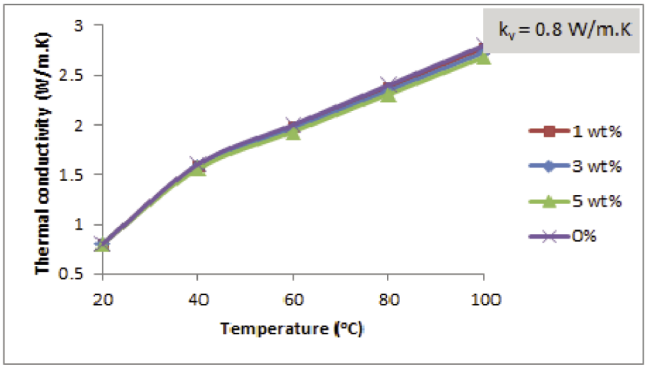

d. X_c=70% & k_v=0.8 W/m.K

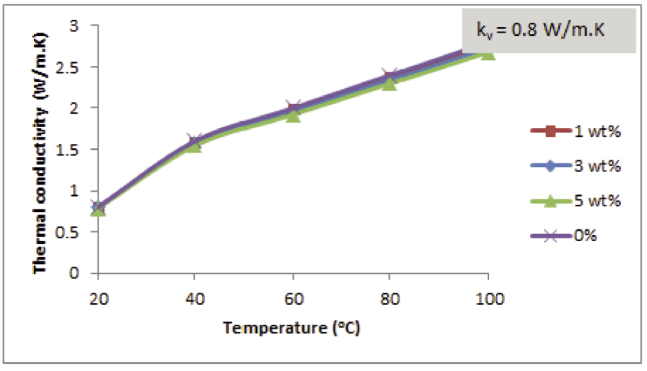

d. X_c=60% & k_v=0.8 W/m.K

Fig. 2 Overall thermal conductivity of perovskite cell at different PA concentrations
2. ábra Perovszkit cella teljes hővezető képessége különböző PA koncentrációk mellett

Fig. 3 Overall thermal conductivity of perovskite cell contains at PT concentrations
3. ábra A perovszkit cella teljes hővezető képessége PT koncentrációban

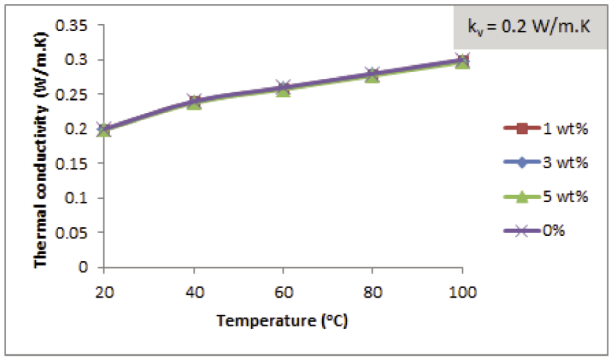

a. X_c=3% & k_v=0.2 W/m.K

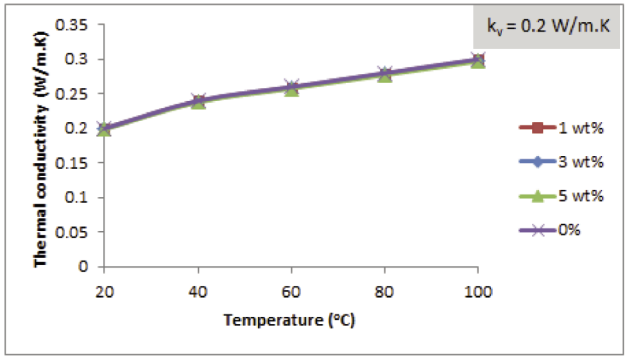

b. X_c=8% & k_v=0.2 W/m.K

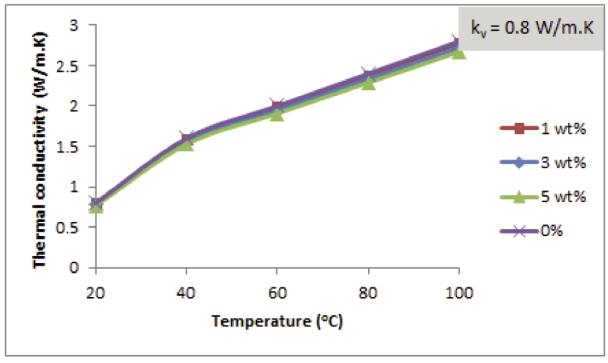

c. X_c=3% & k_v=0.8 W/m.K

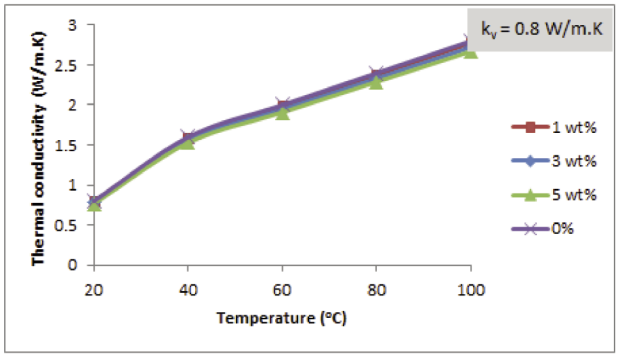

d. X_c=8% & k_v=0.8 W/m.K

Fig. 4 Overall thermal conductivity of perovskite cell at different PS concentrations
4. ábra Perovszkit cella teljes hővezető képessége különböző PS koncentrációk mellett

For validation purpose, the current results can be compared with that obtained from certain studies that may help to understand the differences, as shown in *Table 3*.

Study	Added polymers and loadings	Results
Current	PEO, PA, PT, PS and PMMA 1-5% wt.	The addition of PEO to the perovskite makes the overall k-value higher by 2-3 times, and it is reliable for any temperature rise. In the case of using polymers PA and PT, the overall k-value has fair effects. The use of PS and PMMA has no significant effects.
[16]	PFN, PMMA and PS 1-3% wt.	The addition of polymers enhances the crystalline growth. This leads to improve the thermal conduction. Results shown that increasing the amount of PMMA and PS is not required due to very large size aggregates and non-uniform structure, which leads to less ordered crystalline chains.
[17]	PEO 1% wt.	The addition of PEO enhances the power efficiency by 25%. This is satisfies better thermal conduction.
[18]	PEI 1% wt.	The addition of PEI improves the crystallinity of the film, as well as enhances the power efficiency by 26%. This leads to improve the thermal conduction.
[23]	PVP 3% wt.	The addition of PVP improves the crystallinity of the film, as well as enhances the power efficiency by 30%. This leads to improve the thermal stability and thermal conduction.
[70]	N/A	The k-value kept between 0.3-0.4 W/m·K up to 150 °C.
[71]	N/A	The k-was kept between 0.25-1.0 W/m·K up to 100 °C with a drop in the inclination.
[75]	Theoretical approach	At elevated temperatures up to 54 °C, the k-value was 0.14 W/m·K for the iodine-based perovskite film, and 0.08 W/m·K for the chlorine-based perovskite film.

Table 3 Comparison with certain studies
3. táblázat Összehasonlítás egyes tanulmányokkal

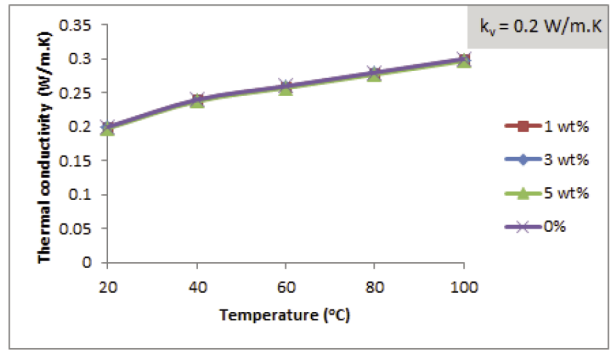

a. X_c=0% & k_v=0.2 W/m.K

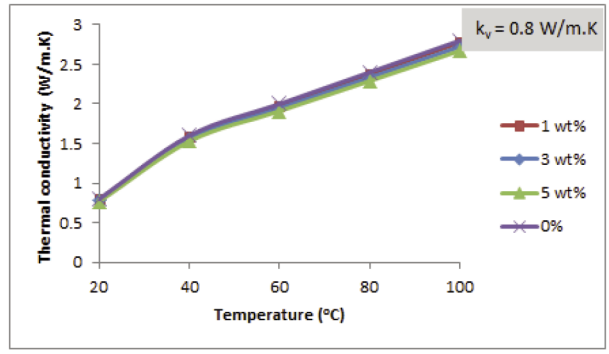

b. X_c=0% & k_v=0.8 W/m.K

Fig. 5 Overall thermal conductivity of perovskite cell at different PMMA concentrations
5. ábra Perovszkit cella teljes hővezető képessége különböző PMMA koncentrációk mellett

4. Conclusions

The study linked the impact of changing the thermal conductivity of some common polymeric additives due to temperature rise on the effective thermal conductivity of the overall perovskite film. The obtained results by the calculations yield the following conclusions:

- In general, polymeric additives may have positive or negative contributions on the final value of the thermal conductivity of the film based on the factors: *k*-value of the perovskite-based material, *k*-value of the polymer and concentration of the polymer.
- Polymers affect thermally when the perovskite-based material is low (0.2 W/m·K) rather than with high *k*-value perovskite material (0.8 W/m·K).
- The existence of PEO within the perovskite-based materials makes the overall *k*-value of the film high at any range of temperatures or polymeric concentrations.
- The overall *k*-value of the film involved PA and PT was less sensitive to the thermal behavior of the polymeric materials, especially at the high design *k*-value (0.8 W/m·K).
- The overall *k*-value of the film has not affected essentially by the adding of amorphous polymers (PS and PMMA).
- There is no significant influence of the degree of crystallinity of the polymer on the overall thermal conductivity of film.

Acknowledgments

Authors are grateful to Materials Engineering Department (Mustansiriyah University) and Mechanical Engineering Department (University of Technology) for facilitating the work.

References

[1] Kalkman J., Bose S., Merhaba A., Bradley H., Emerging technologies in solar PV: identifying and cultivating potential winners, Arthur D. Little, 2015

[2] Manser S., Christians A., Kamat V., Intriguing optoelectronic properties of metal halide perovskites, Chemical Reviews, 116, 21, 12956–13008, 2016. doi:10.1021/acs.chemrev.6b00136

[3] Kojima A., Teshima K., Shirai Y., Miyasaka T., Organometal halide perovskites as visible-light sensitizers for photovoltaic cells, Journal of the American Chemical Society, 131, 17, 6050–6051, 2009. https://doi.org/10.1021/ja809598r

[4] NREL, Best Research-Cell Efficiencies, National Renewable Energy Laboratory, Retrieved 19-08-2022.

[5] Min H., Lee Y., Kim J., Kim G., Lee S., Kim J., Paik J., Min J., Kim K., Kim S., Kim G., Shin J., Il S., Perovskite solar cells with atomically coherent interlayers on SnO2 electrodes, Nature, 598, 7881, 444–450, 2021. https://doi.org/10.1038/s41586-021-03964-8

[6] Roy P., Sinha N., Tiwari S., Khare A., A review on perovskite solar cells: Evolution of architecture, fabrication techniques, commercialization issues and status, Solar Energy, 198, 665–688, 2020.

[7] Eperon G., Burlakov V., Docampo P., Goriely A., Snaith H., Morphological control for high performance, solution-processed planar heterojunction perovskite solar cells, Adv. Funct. Mater., 24, 151–157, 2014.

[8] Shen Q., Ogomi Y., Chang J., Toyoda T., Fujiwara K., Yoshino K., Sato K., Yamazaki K., Akimoto M., Kuga Y., Katayamad K., Hayase S., Optical absorption, charge separation and recombination dynamics in Sn/Pb cocktail perovskite solar cells and their relationships to photovoltaic performances, J. Mater. Chem. A, 3, 9308–9316, 2015.

[9] Salim T., Sun S., Abe Y., Krishna A., Grimsdale A., Lam Y., Perovskite-based solar cells: Impact of morphology and device architecture on device performance, J. Mater. Chem. A, 3, 8943–8969, 2015.

[10] Nie W., Tsai H., Asadpour R., Blancon J., Neukirch A., Gupta G., Crochet J., Chhowalla M., Tretiak S., Alam M., Wang H., Mohite A., High-effciency solution-processed perovskite solar cells with millimeter-scale grains, Science, 347, 522–525, 2015.

[11] Xiao M., Huang F., Huang W., Dkhissi Y., Zhu Y., Etheridge J., Gray-Weale A., Bach U., Cheng Y., Spiccia L., A fast deposition-crystallization procedure for highly efficient lead iodide perovskite thin-film solar cells. Angew. Chem. Int. Ed. Engl, 53, 37, 9898–9903, 2014.

[12] Wenjing H., Yaoming X., Gaoyi H., Jeng-Yu L., The Applications of Polymers in Solar Cells: A Review, Polymers, 11, 143, 2019. https://doi.org/10.3390/polym11010143

[13] Tripathi N., Shirai Y., Yanagida M., Karen A., Miyano K., Novel surface passivation technique for low-temperature solution-processed perovskite PV cells, ACS Appl. Mater. Interfaces, 8, 4644–4650, 2016.

[14] Li T., Pan Y., Wang Z., Xia Y., Chen Y., Huang W., Additive engineering for highly efficient organic-inorganic halide perovskite solar cells: Recent advances and perspectives, J. Mater. Chem. A, 5, 12602–12652, 2017.

[15] Gnida P., Amin M., Pajak A., Jarzabek B., Polymers in high-efficiency solar cells: The latest reports, Polymers, 14, 1946, 2022.

[16] Masi S., Rizzo A., Aiello F., Balzano F., Uccello-Barretta G., Listorti A., Giglia G., Colella S., Multiscale morphology design of hybrid halide perovskites through a polymeric template, Nanoscale, 7, 18956–18963, 2015.

[17] Chang C., Chu C., Huang Y., Huang C., Chang S., Chen C., Chao C., Su W., Tuning perovskite morphology by polymer additive for high efficiency solar cell, ACS Appl. Mater. Interfaces, 7, 4955–4961, 2015.

[18] Dong Q., Wang Z., Zhang K., Yu H., Huang P., Liu X., Zhou Y., Chen N., Song B., Easily accessible polymer additives for tuning the crystal-growth of perovskite thin-films for highly efficient solar cells, Nanoscale, 8, 5552–5558, 2016.

[19] Bi D., Yi C., Luo J., Décoppet J., Zhang F., Zakeeruddin S., Li X., Hagfeldt A., Grätzel M., Polymer-templated nucleation and crystal growth of perovskite films for solar cells with efficiency greater than 21%, Nat. Energy, 1, 16142, 2016.

[20] Kim H., Yusoff A., Jang J., Polystyrene enhanced crystallization of perovskites towards high performance solar cells, Nanoscale Adv., 1, 76–85, 2019.

[21] Xue Q., Hu Z., Sun C., Chen Z., Huang F., Yip H., Cao Y., Metallohalide perovskite-polymer composite film for hybrid planar heterojunction solar cells, RSC Adv., 5, 775–783, 2015.

[22] Zuo L., Guo H., DeQuilettes D., Jariwala S., Marco N., Dong S., DeBlock R., Ginger D., Dunn B., Wang M., Yang Y., Polymer-modified halide perovskite films for efficient and stable planar heterojunction solar cells, Sci. Adv., 3, e1700106, 2017.

[23] Guo Y., Shoyama K., Sato W., Nakamura E., Polymer stabilization of lead(II) perovskite cubic nanocrystals for semitransparent solar cells, Adv. Energy Mater., 6, 1502317, 2016.

[24] Chaudhary B., Kulkarni A., Jena A., Ikegami M., Udagawa Y., Kunugita H., Ema K., Miyasaka T., Poly(4-Vinylpyridine)-based interfacial passivation to enhance voltage and moisture stability of lead halide perovskite solar cells, ChemSusChem, 10, 2473–2479, 2017.

[25] Wang Y., Luo J., Nie R., Deng X., Planar perovskite solar cells using CH3NH3PbI3 films: A simple process suitable for large-scale production, Energy Technol., 4, 473–478, 2016.

[26] Zhao Y., Wei J., Li H., Yan Y., Zhou W., Yu D., Zhao Q., A polymer scaffold for self-healing perovskite solar cells, Nat. Commun., 7, 10228, 2016.

[27] Wang F., Shimazaki A., Yang F., Kanahashi K., Matsuki K., Miyauchi Y., Takenobu T., Wakamiya A., Murata Y., Matsuda K., Highly efficient and stable perovskite solar cells by interfacial engineering using solution-processed polymer layer, J. Phys. Chem. C, 121, 1562–1568, 2017.

[28] Ji X., Peng X., Wang Q., Ren J., Xiong Z., Yang X., On the performance of polymer:organometal halide perovskite composite light emitting devices: The effects of polymer additives, Org. Electron., 52, 350–355, 2018.

[29] Jiang J., Lang X., Zeng Q., Faheem M., Rong S., Zhao H., Li Y., Polyacetylene derivatives in perovskite solar cells: from defect passivation to moisture endurance, Journal of Materials Chemistry A, Issue 22, 2021.

[30] Yan W., Li Yu., Sun W., Peng H., Ye S., Liu Z., Bian Z., Huanga C., High-performance hybrid perovskite solar cells with polythiophene as hole-transporting layer via electrochemical polymerization, RSC Advances, Issue 62, 2014.

[31] Yan W., Li Y., Li Yu, Ye S., Liu Z., Wang S., Bian Z., Huang C., High-performance hybrid perovskite solar cells with open circuit voltage dependence on hole-transporting materials, Nano Energy, Volume 16, Pages 428-437, 2015.

[32] Fried J., Polymer science and technology, 3rd ed., Prentice Hall, 2014.
[33] Ebewele R., Polymer science and technology, 1st ed., CRC Press, 2000.
[34] Krevelen D., Nijenhuis K., Properties of polymers, 4th ed., Elsevier, 2009.
[35] Ehrenstein G., Polymeric Materials: Structure, Properties, Applications, 1st ed., Hanser Verlag, 2001.
[36] Jia Y., Mao Z., Huang W., Zhang J., Effect of temperature and crystallinity on the thermal conductivity of semi-crystalline polymers: A case study of polyethylene, Materials Chemistry and Physics, Volume 287, 126325, 2022. https://doi.org/10.1016/j.matchemphys.2022.126325
[37] Guo B., Lin Q., Zhao X., Zhou X., Crystallization of polyphenylene sulfide reinforced with aluminum nitride composite: effects on thermal and mechanical properties of the composite, Iran, Polym. J., 24, 965–975, 2015. https://doi.org/10.1007/s13726-015-0385-5
[38] Robbins A., Minnich A., Crystalline polymers with exceptionally low thermal conductivity studied using molecular dynamics, Appl. Phys. Lett., 107, 201908, 2015.
[39] Yu J., Sundqvist B., Tonpheng B., Andersson O., Thermal conductivity of highly crystallized polyethylene, Polymer, 55, 195–200, 2014.
[40] Ruiz-Reina E., Sidrach-de-Cardona M., Piliougine M., Heat Transfer and Working Temperature Field of a Photovoltaic Panel Under Realistic Environmental Conditions, 2019. Available on: https://www.comsol.com/paper/download/199363/ruizreina_abstract.pdf
[41] Hameed R., Mathematical model to investigate the temperature distribution for photovoltaic panels, Journal of University of Babylon for Engineering Sciences, Vol. 26, No. 8, 2018.
[42] Gaitho F., Ndiritu F., Muriithi P., Ngumbu R., Ngareh J., Effect of thermal conductivity on the efficiency of single crystal silicon solar cell coated with an anti-reflective thin film, Solar Energy, Volume 83, Issue 8, 1290-1293, 2009. https://doi.org/10.1016/j.solener.2009.03.003
[43] Pavlovic A., Fragassa C., Bertoldi M., Mikhnych V., Thermal Behavior of Monocrystalline Silicon Solar Cells: A Numerical and Experimental Investigation on the Module Encapsulation Materials, J. Appl. Comput. Mech., 7, 3, 1847-1855, 2021. https://doi.org/10.22055/JACM.2021.37852.3101
[44] Jeong W., Min J., Kim H., Kim J., Kim J., Lee D., Influence of effective thermal conductivity on the performance of the highly efficient CZTSSe thin film solar cells, IEEE 7th World Conference on Photovoltaic Energy Conversion (WCPEC) (A Joint Conference of 45th IEEE PVSC, 28th PVSEC & 34th EU PVSEC), pp. 1893-1896, 2018. https://doi.org/10.1109/PVSC.2018.8547943.
[45] Ilahi S., Almosni S., Chouchane F., Perrin M., Zelazna K., Yacoubi N., Kudrawiec R., Râle P., Lombez L., Guillemoles J., Durand O., Cornet C., Optical absorption and thermal conductivity of GaAsPN absorbers grown on GaP in view of their use in multijunction solar cells, Solar Energy Materials and Solar Cells, 141, 291-298, 2015. https://doi.org/10.1016/j.solmat.2015.06.003
[46] Polaskova M., Peer P., Cermak R., Ponizil P., Effect of thermal treatment on crystallinity of poly(ethylene oxide) electrospun fibers, Polymers, 11, 1384, 2019.
[47] Wen X., Su Y., Li S., Ju W., Wang D., Isothermal crystallization kinetics of poly(ethylene oxide)/poly(ethylene glycol)-g-silica nanocomposites, Polymers, 13, 648, 2021.
[48] Meng H., Yu X., Feng H., Xue Z., Yang N., Superior thermal conductivity of poly (ethylene oxide) for solid-state electrolytes: A molecular dynamics study, International Journal of Heat and Mass Transfer, Volume 137, Pages 1241-1246, 2019.
[49] Akaishi T., Miyasaka K., Ishikawa K., Shirakawa H., Ikeda S., Crystallinity of bulk polyacetylene, Journal of Polymer Science: Polymer Physics Edition, Volume 18, Issue 4, Pages 745-750, 1980.
[50] Belov D., Efimov O., Belov G., Synthesis, Properties, and Applications of Polyacetylene and Polyacetylene-Based Composites, in the book: Electrical and Optical Polymer Systems, 1st ed., CRC Press, 1998.
[51] Zhang T., Wu X., Luo T., Polymer nanofibers with outstanding thermal conductivity and thermal stability: fundamental linkage between molecular characteristics and macroscopic thermal properties, J Phys Chem C, 118, 21148–21159, 2014.
[52] Shen X., Hu W., Russell T., Measuring the degree of crystallinity in semicrystalline regioregular poly(3-hexylthiophene), Macromolecules, 49, 12, 4501–4509, 2016.
[53] Youm S., Hwang E., Chavez C., Li X., Chatterjee S., Lusker K., Lu L., Strzalka J., Ankner J., Losovyj Y., Garno J., Nesterov E., Polythiophene thin films by surface-initiated polymerization: mechanistic and structural studies, Chem. Mater., 28, 13, 4787–4804, 2016.
[54] Brun N., Bourson P., Margueron S., Duc M., Study of the thermal behavior of syndiotactic and atactic polystyrene by Raman spectroscopy, JEEP, 00004, 2011.
[55] Simpson A., Rattigan I., Kalavsky E., Parr G., Thermal conductivity and conditioning of grey expanded polystyrene foams, Cellular Polymers, Vol. 39, 6, 238–262, 2020.
[56] Mathur V., Sharma K., Thermal response of polystyrene/poly methyl methacrylate (PS/PMMA) polymeric blends, Heat Mass Transfer, 52, 2901–2911, 2016.
[57] Lin T., Li Y., Wang J., You J., Effect of PMMA molecular weight on its localization during crystallization of PVDF in their blends, Polymers, 13, 23, 4138, 2021.
[58] Elimat Z., Zihlif A., Avella M., Thermal and optical properties of poly(methyl methacrylate)/calcium carbonate nanocomposite, Journal of Experimental Nanoscience, 3:4, 259-269, 2008.
[59] Tawfeeq W. Mohammed, Insulation Materials: Principles and Applications, 1st ed., Mustansiriyah University, 2021.
[60] Hung Anh L., Pásztory Z., An overview of factors influencing thermal conductivity of building insulation materials, Journal of Building Engineering, 44, 2021. https://doi.org/10.1016/j.jobe.2021.102604.
[61] Dos Santos W., De Sousa J., Gregorio R., Thermal conductivity behaviour of polymers around glass transition and crystalline melting temperatures, Polymer Testing, 32, 987–994, 2013.
[62] Hongyu C., Valeriy G., Jian Y., Yunfeng Y., Wei L., Yan H., Libo D., Bin C., Thermal conductivity of polymer-based composites: Fundamentals and applications, Progress in Polymer Science, 59, 41-85, 2016.
[63] Zarandi M., Bioki H., Mirbagheri Z., Tabbakh F., Mirjalili G., Effect of crystallinity and irradiation on thermal properties and specific heat capacity of LDPE & LDPE/EVA. Applied Radiation and Isotopes, 70, 1–5, 2012.
[64] Zinet M., Refaa Z., Boutaous M., Xin S., Bourgin P., Thermophysical characterization and crystallization kinetics of semi-crystalline polymers, Journal of Modern Physics, 4, 2013.
[65] Bai L., Zhao X., Bao R., Liu Z., Yang M., Yang W., Effect of temperature, crystallinity and molecular chain orientation on the thermal conductivity of polymers: a case study of PLLA, J. Mater Sci, 53, 10543–10553, 2018.
[66] Zaki N., Experimental and Theoretical Investigation to Study the Effect of Crystallinity on the Thermal Properties of Polymers, MSc Thesis, University of Mustansiriyah, Iraq, 2021.
[67] Haeger T., Heiderhoff R., Riedl T., Thermal properties of metal-halide perovskites, J. Mater. Chem. C, 8, 14289-14311, 2020.
[68] Hu Z., Aigouy L., Chen Z., Fournier D., Thermal conductivity and diffusivity of triple-cation perovskite halide materials for solar cells, Journal of Applied Physics, 127, 125113, 2020.
[69] Osei-Agyemang E., Adu C., Balasubramanian G., Ultralow lattice thermal conductivity of chalcogenide perovskite CaZrSe3 contributes to high thermoelectric figure of merit, npj Comput Mater, 5, 116, 2019. https://doi.org/10.1038/s41524-019-0253-5
[70] Ye T., Wang X., Li X., Yan A., Ramakrishna S., Xu J., Ultra-high Seebeck coefficient and low thermal conductivity of a centimeter-sized perovskite single crystal acquired by a modified fast growth method, J. Mater. Chem. C, 5, 1255-1260, 2017.
[71] Lee W., Li H., Wong A., Zhang D., Lai M., Yu Y., Kong Q., Lin E., Urban J., Grossman J., Yang P., Ultralow thermal conductivity in all-inorganic halide perovskites, PNAS, vol. 114, no. 33, 8693–8697, 2017.
[72] Chen Q., Zhang C., Zhu M., Liu S., Siemens M., Gu S., Zhu J., Shen J., Wu X., Liao C., Zhang J., Wang X., Xiao M., Efficient thermal conductance in organometallic perovskite CH3NH3PbI3 films, Appl. Phys. Lett., 108, 081902, 2016. https://doi.org/10.1063/1.4942779
[73] Haeger T., Heiderhof R., Riedl T., Thermal properties of metal-halide perovskites, J. Mater. Chem. C, 8, 14289, 2020.
[74] Oltulu O., Ozer Z., Mamedov A., Ozbay E., Band structures of metacompsosite based phononic crystals in quasi-Sierpinski fractals, Építőanyag–Journal of Silicate Based and Composite Materials, Vol. 74, No. 2 (2022), 57–60. p. https://doi.org/10.14382/epitoanyag-jsbcm.2022.9
[75] Aleksandrova M., Pandiev I., Singh A., Implementation of 3ω method for studying the thermal conductivity of perovskite thin films, Crystals, 12, 1326, 2022.

Ref.:
Mohammed, Tawfeeq W. – **Al-Ghezi**, Moafaq K.S. – **Atea**, Ibrahim A.: *The effect of temperature rise on the thermal conductivity of composite (perovskite/polymer) solar cell*
Építőanyag – Journal of Silicate Based and Composite Materials, Vol. 75, No. 2 (2023), 67–74. p.
https://doi.org/10.14382/epitoanyag-jsbcm.2023.10

Performance assessment of adsorbents based on natural bentonite for removal of cationic dye

Mazouri BELHADRI ▪ Laboratory of Rheology, Transport and Treatment of the Complex Fluids, Faculty of Architecture and Civil Engineering, University of Science and Technology of Oran Mohamed Boudiaf (USTO-MB), Algeria
Abdelkader BENGUEDDACH ▪ Laboratory of Chemistry of Materials L.C.M, Department of Chemistry, Faculty of Exact and Applied Sciences, University of Oran1 Ahmed Ben Bella, Algeria
Mohamed SASSI ▪ Laboratory of Chemistry of Materials L.C.M, Department of Chemistry, Faculty of Exact and Applied Sciences, University of Oran1 Ahmed Ben Bella, Algeria
Érkezett: 2022. 11. 29. ▪ Received: 29. 11. 2022. ▪ https://doi.org/10.14382/epitoanyag-jsbcm.2023.11

Abstract
The development of safe and cost-effective methods for the treatment of dye polluted wastewater has been a great concern. Herein, Adsorption of methylene blue from aqueous solutions onto modified clay has been investigated. Three adsorbants were prepared through the treatment of a natural Algerian bentonite (NAB) by sodium (Na-Clay), calcium (Ca-Clay), and sulfuric acid solution (Hs-Clay), respectively. The accomplished materials was performed by X-ray diffraction and Fourier transforminfrared (FTIR).
The effects of differents process parameters such as contact time, pH of dye solution, initial concentration of dye, and adsorbent amount on the removal efficiency of methylene blue (MB) from aqueous solution were evaluated by batch experiment. The maximum adsorption capacity of 220.28 mg/g reached by Na-Clay. Furthermore, all the prepared adsorbents also displayed a prominent efficiency in removal of cationic dyes.
The findings reveal the feasibility of facile clay modification to be used as a potential and rapid low cost adsorbent for removal of cationic dyes from wastewater.
Keywords: clay, water pollution, adsorption, methylene blue, isotherms
Kulcsszavak: agyag, vízszennyezés, adszorpció, metilénkék, izotermák

Mazouri BELHADRI
PhD, Hydraulic Department, Faculty of Architecture and Civil Engineering, University of Science and Technology of Oran Mohamed Boudiaf (USTO-MB), Algeria.
Fields of interests: rheology, pollution, water treatment, clays, valorization of solid waste.

Abdelkader BENGUEDDACH
Professor, Department of Chemistry, Faculty of Exact and Applied Sciences, Université d'Oran 1 Ahmed Ben Bella, Algeria.
Former director of materials chemistry laboratory
Fields of interests: clay, zeolite, catalysis, adsorption.

Mohamed SASSI
Professor, Department of Chemistry, Faculty of Exact and Applied Sciences, Université d'Oran 1 Ahmed Ben Bella, Algeria.
Director of materials chemistry laboratory
Fields of interests: chemistry, material chemistry, nanomaterials and applications

1. Introduction

Water pollution has become a serious global problem due to rapid industrialization and various human activities. Dyes effluents, originating from dyeing, textile, leather, paper and other related industries, are one of the most severe environmental pollutants because of their high toxicity to plants [1], aquatic life [2–4] and human beings [5–7]. Consequently, it is of significance to treat colored wastewater prior to their discharge into natural environment. For this reason, many attempts such as membrane separation, flocculation precipitation, oxidation, photocatalytic, degradation, microbial degradation, and adsorption have been studied for the removal of dyes from wastewater [8]. Among them, adsorption has been widely regarded as one of the most efficient treatments for dyes in wastewater due to its cost effective operation, simple and diverse design, and high efficiency [9–10].

Number of natural adsorbents have been used for the removal of pollutants from water [11]. Utilization of clays as adsorbents could bring great economical and environmental benefits to wastewater industries compared to synthesized materials [12]. Previous works reported that the utilization of clays as adsorbents was efficient for the removal of dyes [13; 15].

In order to improve the adsorption properties of raw bentonite, the modification of mineral clay was attractive for researchers, numerous studies have investigated MB removal from aqueous solution, using clay modified with dodecyl sulfobetaine surfactant [15] poly(acrylic acid-co-2-acrylamido-2-methylpropanesulfonic acid) hydrogel nanocomposite [16], Fe_3O_4 [17]. Another potential candidate for a MB sorbent is sodium or calcium-exchanged and acid-activated bentonite, where their preparation is relatively inexpensive and easy compared with that of other modifications of bentonite which can cause secondary pollution due to the leaching of modifying agents.

The main objective of this paper was to obtain several low-cost and very efficient adsorbents based on local clay which is a bentonite, a clay mineral of the smectite group having silica tetrahedral sheets layered between alumina octahedral sheets. The adsorbent materials realized were characterized and used in investigated to remove methylene blue from synthetic wastewater. The effects of initial pH value, adsorbent dosage, initial MB concentration, and contact time were checked. Furthermore, adsorption isotherms were investigated.

2. Experimental

2.1 Materials and methods

All the reagents were of analytical grade and used as received. A stock solution of dye having a concentration of 1000 mg/L was prepared by dissolving appropriate amount of MB dye powder in 1 L deionized water and then it was diluted to the desired concentration of each experiment. The molecular formula of MB dye is $C_{16}H_{18}ClN_3S$ with the molecular weight of 319.851 g/mol.

Our supports have been characterized by X-ray diffraction and The Fourier transform infrared (FTIR). A Phillips Analytical X-ray spectrometer (PW 1830) using CuKα radiation was used to characterize the adsorbents. FTIR spectra of the adsorbents were taken with a Perkin Elmer 1600 Spectrometer (range 4000–400 cm^{-1}). The UV/VIS (V-670) spectrophotometer was used to measure the concentration of MB dye in solution at wave length of λ_{max} = 665 nm. The pH solution was adjusted using reagent grade HCl and NaOH.

2.2 Adsorbents

Natural bentonite (NAB) from Maghnia deposit in west of Algeria, was used without any chemical pretreatment to produce three modified clay adsorbents. Na-Clay and Ca-Clay were obtained by treating the NAB sample for four hours with a solution of NaCl (0.5 M) and a solution of $CaCl_2$ (0.5 M), respectively. The mixtures were filtered, washed with distilled water until Cl^- ions were not detected by the silver nitrate test and then air-dried at room temperature. Afterwards, NAB was treated under reflux for two hours with an aqueous H_2SO_4 solution (10 wt. %). The suspension obtained was filtered and the solid resulting, named (Hs-Clay), was washed with distilled water until it was free of SO_4^{2-} ($BaCl_2$ test) and then air-dried at room temperature.

2.3 Adsorption experiments

All the adsorption experiments were conducted in triplicate under the same conditions. The effect of various parameters on the adsorption behaviour of the adsorbents (NAB, Na-Clay, Ca-Clay and Hs-Clay) were studied. The experimental variables examined were contact time, bentonite concentration in suspension, pH of suspension and MB concentration. Suspensions of solid adsorbents and MB adsorbate solutions were obtained by contacting 0.1 g of dry NAB, Na-Clay, Ca-Clay and HS-Clay solid adsorbents with 100 mL of 80 mg/L of MB solutions separately in sealed Erlenmeyer flasks. The mixtures obtained were magnetically stirred at room temperature at different time intervals (0–120 min). After that, the flasks were centrifuged and the concentration of MB in aqueous solution was determined by UV–VIS spectrophotometer. The effect of pH solution on MB adsorption was investigated in a pH range between 3 and 10. In these cases, the pH value of the solution was adjusted to the desired value by adding HCl or NaOH as required. Batch sorption experiments were also conducted to reveal the effect of adsorbent the amount on the removal of MB from aqueous solution. The effect of adsorbent dose was varied from 0.25 g up to 4.0 g. To establish the adsorption isotherms, this study was carried out with different initial MB concentrations varying from 5 mg/L to 280 mg/L. The adsorbent MB uptake, per unit mass of clay at time t, q_t (mg/g) was evaluated by the following equations:

$$q_t = (C_0 - C_t)\frac{V}{m} \quad (1)$$

$$q_e = (C_0 - C_e)\frac{V}{m} \quad (2)$$

Where q_t and q_e (mg/g) are adsorption amount of the dye at time t and equilibrium, C_0, C_t and (mg L^{-1}) are the concentration of MB solution at initial, time t and equilibrium, respectively, V (L) is the volume of MB solution and m (g) corresponds to dosage of adsorbent.

3. Results and discussion

3.1 Characterizations

Fig. 1 presents the X-ray diffraction patterns of natural bentonite (NAB), Na-Clay, Ca-Clay and Hs-Clay samples. The X-ray diffraction pattern of NAB shows many diffraction peaks from montmorillonite, which is characterized by four peaks: one located at 15.61 Å (d_{001}) and the other three at 4.49 Å (d_{020}), 3.79 Å (d_{004}), and 1.50 Å (d_{060}). Some peaks were identified as impurities (Quartz, calcite, cristabolite, hematite and dolomite). The results relating to the identification of the minerals present in NAB are summarized in the *Table 1*.

Clay, Basal spacing (Å)	Impurities, Basal spacing d (Å)				
Montmorillonite	Quartz	Cristabolite	Dolomite	Calcite	Hematite
15.61 (001)	3.36	3.23	2.22	3.04	2.71
4.49 (020)	1.54			2.29	1.87
3,79 (004)	1.38			1.91	1.60
2.56 (200)					
1.50 (060)					
1.69 (009)					

Table 1 Intereticular distances of different NAB minerals (Å) according to X-ray diffraction analysis
1. táblázat Különböző NAB ásványok interetikuláris távolságai (Å) röntgendiffrakciós elemzés szerint

Compared with NAB clay, as shown in *Fig. 1*, the basal spacing (d_{001}) of Na-Clay decreases from 15.61 Å to 12.91 Å as a consequence of the ion exchange process. Similar observations have also been reported by other authors [18]. In contrast, the basal spacing d_{001} of Ca-Clay and Hs-Clay expanded to 15.75 Å and 16.19 Å, respectively. Indicating that ion exchange did take place.

The FTIR spectra of samples NAB, Na-Clay, Ca-Clay and Hs-Clay are depicted in Fig. 2. The absorption band observed at 3510 cm^{-1} is attributed to hydroxyl group vibrations of Mg–OH–Al, Fe–OH–Al and Al–OH–Al units in the octahedral layer, typical of montmorillonite [19, 20]. The very broad vibration band at 3388 cm^{-1} is due to the O–H stretching vibration of the interlayer silanol (Si–OH) groups and also to the HO–H vibration of the interlayer water adsorbed silica surface involved in hydrogen bonding linkages. The absorption band at 1632 cm^{-1} is attributed to the vibration of physisorbed water molecules. The band near 1100 cm^{-1} is attributed to stretching vibration of the Si–O–Si groups of the tetrahedral layer. The broad band at 977 cm^{-1} is related to the stretching vibrations of the Si–O groups. It is observed that the samples display all the absorption bands of the parent NAB material, indicating that the layered structure is preserved after modification.

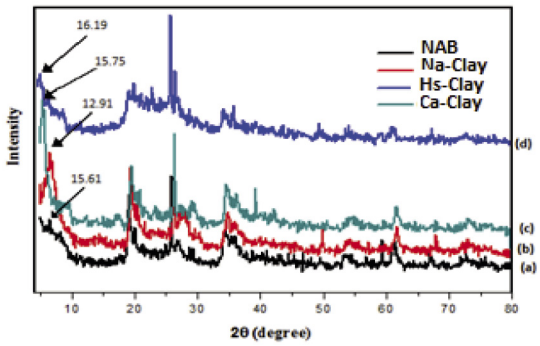

Fig. 1 X-ray diffraction patterns of NAB (a), Na-Clay (b), Ca-Clay (c), and Hs-Clay (d) samples
1. ábra NAB (a), Na-agyag (b), Ca-agyag (c) és Hs-agyag (d) minták röntgendiffrakciós mintázata

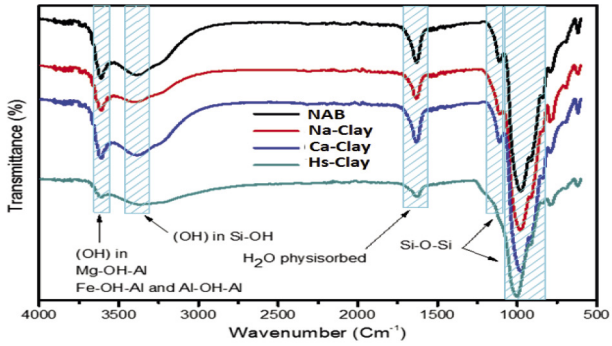

Fig. 2 FTIR spectra of NAB (a), Na-Clay (b), Ca-Clay (c), and Hs-Clay (d) samples
2. ábra NAB (a), Na-agyag (b), Ca-agyag (c) és Hs-agyag (d) minták FTIR spektruma

3.2 Adsorption

3.2.1 Effet of contact time

It is known that the performance of dye removal from aqueous solution is significantly affected by contact time. As shown in *Fig. 3*, it was apparent that the adsorption capacity rapidly increased at beginning and then gradually slowed down until equilibrium. This may be ascribed to the higher MB concentration and abundant free adsorption sites available at initial adsorption phase [22].

It is noted that a contact time of only 10 min is sufficient to reach equilibrium when Na-Clay and Ca-Clay adsorbents are used, while a contact time of 40 min is necessary in the case of Hs-Clay solid.

3.2.2 Effect of pH

The influence of pH solution on the removal of MB by modified bentonite was investigated to gain further insight into the adsorption process. *Fig. 4* shows the qe of NAB, Na-Clay, Ca-Clay and Hs-Clay in various pH solutions. The absorption capacity of Hs-Clay for MB was much lower than that of Na-Clay and Ca-Clay. While the qe values of Na-Clay were greater than those of Ca-Clay in the range pH 3–10. On the other hand, the qe values of adsorbents increased with the increase of pH solution, which also could be explained by the electrostatic interaction of positive charges of MB with the negative charges of clay, which were enhanced at higher pH values, leading to greater q_e values. The adsorption was not drastically affected by pH, suggesting the presence of other interactions (such as hydrophobic interaction) between MB and adsorbents Similar observations have also been reported by other authors [15]. At the low pH, excess H^+ ions have resulted in the formation of a positive charge on the adsorbent's surface, and it reduces the attractive force between the adsorbent and the cationic MB dyes [23, 24]. The maximum adsorption percentage was observed at pH=7. The same trend has been supported by the literature for MB sorption [24, 25]. Therefore, pH=7 value was selected as optimum pH for MB removal from aqueous solution.

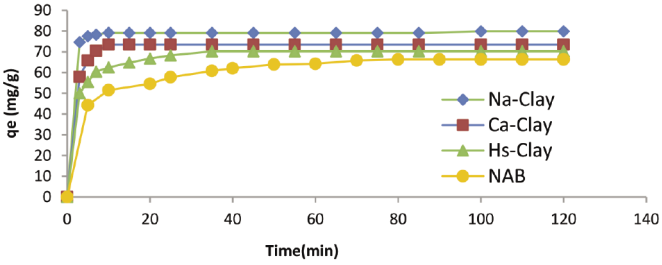

Fig. 3 Kinetics of MB removal onto NAB, Na-Clay, Ca-Clay, and Hs-Clay adsorbents
3. ábra Az MB eltávolításának kinetikája NAB, Na-agyag, Ca-agyag és Hs-agyag adszorbenseken

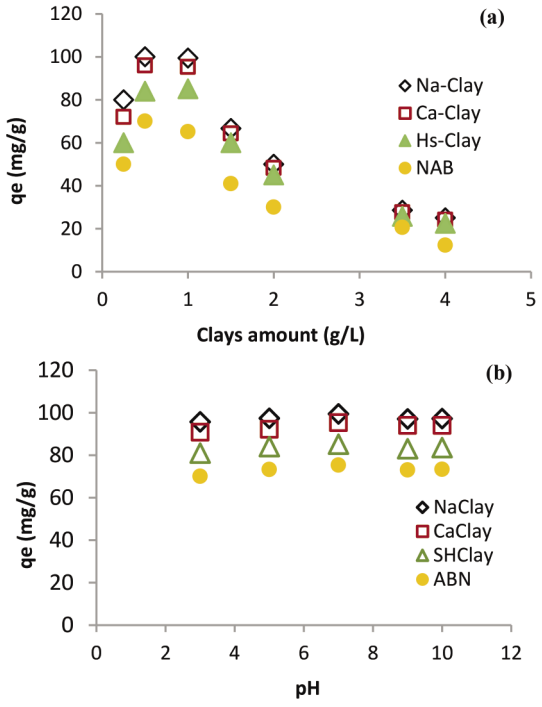

Fig. 4 Effect of Clays amount (a), and pH (b) on sorption of MB onto NAB, Na-Clay, Ca-Clay and Hs-Clay adsorbents
4. ábra Az agyagok mennyiségének (a) és a pH-értéknek (b) a hatása az MB NAB, Na-agyag, Ca-agyag és Hs-agyag adszorbenseken történő szorpciójára

3.2.3 Effect of adsorbent dose

Adsorbent doses are optimized by introducing the various amounts of NAB, Na-Clay, Ca-Clay, and Hs-Clay (0.25 g/L to 4.0 g/L) in the MB dye solution. Maximum amount of dye removal is observed at 1 g/L (fig.4). In contrast, a very slight decrease in removal percentage has been noticed with an increase in the adsorbent dosage. Initially, the removal percentage increases with the adsorbent dosages, as many

active sites are available in the adsorbents. At a high dose, It could be seen that the adsorption capacity of Na-Clay, Ca-Clay, Hs-Clay and NAB decreased with increasing adsorbent dose. These results could be due to the agglomeration of the active sites on the adsorbent surface and the heightened diffusion path length responsible for the reduction in the adsorption capacity [26].

3.2.4 Effect of dye concentration

The adsorption isotherms of MB onto NAB, Na-Clay, Ca-Clay and Hs-Clay are shown in *Fig. 5*. It appears in all cases that the adsorption loading of MB (mg/g) at equilibrium qe increases until a certain limit when increasing the initial concentration of the MB solution; afterward, it remains constant (*Fig. 5*). The adsorbed amounts are 82.35, 220.28, 217.50, 117.14 mg/g respectively for ANB, Na-Clay, Ca-Clay and Hs-Clay. The maximum adsorption capacity is observed in the case of Na-Clay adsorbent. This is attributed to the enhanced swelling property of Na-Clay [26].

Comparison of maximum sorption capacity for MB of different adsorbents

Adsorption capacities (q_m) of various adsorbents towards methylene blue dye as reported in literature were presented in *Table 2*.

A comparison between this work and other reported data from the literature shows that modified bentonite is a better adsorbent for methylene blue compared to other adsorbents. Therefore, it could be safely concluded that the Na-Clay, Ca-Clay and Hs-Clay adsorbents have a considerable potential for the removal of methylene blue from an aqueous solution.

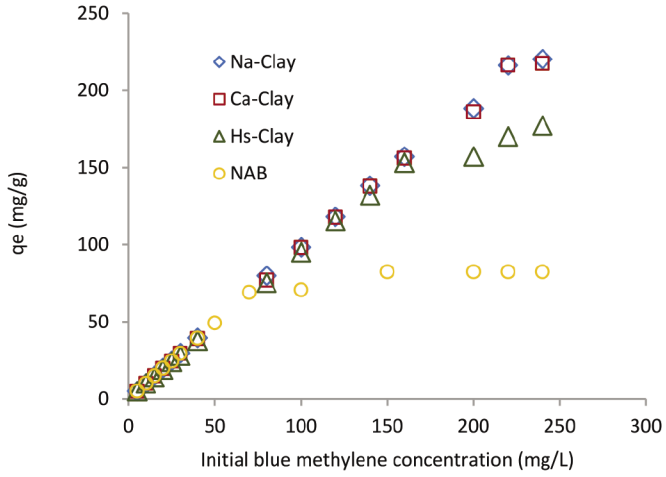

Fig. 5 Isotherms of MB adsorption onto NAB, Na-Clay, Ca-Clay and Hs-Clay adsorbents
5. ábra Az MB adszorpció izotermái NAB, Na-agyag, Ca-agyag és Hs-agyag adszorbenseken

4. Conclusions

In this study, the low-cost modified clays were prepared with different cations, and their performances of the adsorptive removal of MB from wastewater were investigated. All the

Material	pH/ Optimal pH	Contact Time/ equilibrium time (min)°	Concentration (mg/L)	Amount adsorbent	q_m (mg/g)	Ref.
Hydrochloric Acid-modified Rectorite	2-12 / 7	5–90 / 30	20–100	1–8 g/L	37.00	[2]
Black cumin seeds	1-9 / 4.8	5–120 / 20	20–100	0.1 g / 50 ml	16.85	[4]
magnetic halloysite–chitosan nanocomposites	5-11 / 8	0–1440 / 15	20–200	25 mg / 25 ml	50.37	[6]
Purified clay (Na-TIFL)	No indicated	60 / 10	80–200	1 g/L	82.00	[13]
Natural clay	3–12 / 7	0–250 / <50	9–300	1 g/L	100.00	[14]
Dodecyl sulfobetaine surfactant-modified montmorillonite	2–11 / 5	0–120 / 60	0–350	0.05 g /50 mL	254.00	[15]
Poly(AA-co-AMPS)/ montmorillonite nanocomposite hydrogel	2–13 / 10	600	10–150	20–120 mg	215.00	[16]
Fe3O4/activated montmorillonite nanocomposite	3–11 / 7.37	0-60 /	100–250	0.625–2.5 g/L	106.38	[17]
Eco-friendly polyvinyl alcohol/ carboxymethyl cellulose hydrogels reinforced with graphene oxide and bentonite	2-10 / 8	0–250	0–250	30 mg / 20mL	172.14	[21]
Acid-Treated Eucalyptus Leaves	2–10 / 8	5–360	10–300	1–10 g/L	194.34	[22]
NAB	3-10 / 7	0–120	5–280	0.25–4.0 g/L	82.35	This work
Na-Clay	3-10 / 7	0–120	5–280	0.25–4.0 g/L	220.28	This work
Ca-Clay	3-10 / 7	0–120	5–280	0.25–4.0 g/L	217.50	This work
Hs-Clay	3-10 / 7	0–120	5–280	0.25–4.0 g/L	117.14	This work

Table 2 Comparison of the maximum adsorption capacity of MB on some natural and synthetic adsorbents from aqueous solution
2. táblázat Az MB maximális adszorpciós kapacitásának összehasonlítása egyes természetes és szintetikus adszorbenseken, vizes oldatból származó MB esetében

results demonstrate that the three adsorbents can effectively remove cationic dye pollutants, represented by methylene blue. The Na-Clay showed superior adsorption performance compared to Ca-Clay and Hs-Clay. The effects of contact time, initial metal concentration, pH value, and adsorbent mass on the adsorption process were discussed. The results of this study indicate that a simple modification of clay is a reusable adsorbent for the fast and highly efficient removal of MB from aqueous solutions.

References

[1] Moorthy, K. A. – Rathi, B. G. S. – Shukla, S. P. – Kumar, K. –Bharti, V. S. (2021): Acute toxicity of textile dye Methylene blue on growth and metabolism of selected freshwater microalgae, Environmental Toxicology and Pharmacology, 103552. https://doi.org/10.1016/j.etap.2020.103552

[2] Zhang, G. – Liu, G. – Guo, Y. (2011): Adsorption of methylene blue from aqueous solution onto hydrochloric acid-modified rectorite, Journal of Wuhan University of Technology-Mater. Vol. 26, pp. 817–822. https://doi.org/10.1007/s11595-011-0317-y

[3] Singh, N. B. – Nagpal, G. – Agrawal, S. (2018): Water purification by using adsorbents: (review), Environmental Technology & Innovation, Vol. 11 pp. 187–240. https://doi.org/10.1016/j.eti.2018.05.006

[4] Yaseen, D. A. – Scholz, M. (2016): Shallow pond systems planted with Lemna minor treating azo dyes. Ecological Engineering, Vol. 94, pp. 295–305. http://dx.doi.org/10.1016/j.ecoleng.2016.05.081

[5] Rafatullah, M. – Sulaiman, O. – Hashim, R. – Ahmad, A. (2010): Adsorption of methylene blue on low-cost adsorbents (review), Journal of Hazardous Materials, Vol. 177, Issues (1–3), pp. 70–80, https://doi.org/10.1016/j.jhazmat.2009.12.047

[6] Shooto, N .D. – Nkutha, C. S. – Guilande, N. R. – Naidoo, E. B. (2020): Pristine and modified mucuna beans adsorptive studies of toxic lead ions and methylene blue dye from aqueous solution, South African Journal of Chemical Engineering, Vol. 31, pp. 33–43. https://doi.org/10.1016/j.sajce.2019.12.001

[7] Zhou, J. – Lü, Q.-F. – Luo, J.-J. (2017): Efficient removal of organic dyes from aqueous solution by rapid adsorption onto polypyrrole–based composites, Journal of Cleaner Production, Vol. 167, pp. 739–748. doi:10.1016/j.jclepro.2017.08.196

[8] Duan, M. – Wu, J. – Xiong, Y. – Fang, S. – Chen, J. (2018): Characterization and differentiation of the adsorption behavior of crystal violet and methylene blue at the silica/water interface using near field evanescent wave, Soft Matter, Vol. 14, pp. 7516-7525. https://doi.org/10.1039/C8SM01385C

[9] Samadder, R. – Akter, N. – Roy, A. C. – Uddin, M. M. Hossen, M. J. ––Azam, M. S. (2020): Magnetic nanocomposite based on polyacrylic acid and carboxylated cellulose nanocrystal for the removal of cationic dye, RSC Advances, Vol. 10, pp. 11945–11956. https://doi.org/10.1039/D0RA00604A.

[10] Bulut, E. – Özacar, M. – Şengil, İ.A. (2008): Adsorption of malachite green onto bentonite: Equilibrium and kinetic studies and process design, Microporous and Mesoporous Materials, Vol. 11, Issue 3, pp. 234–246. https://doi.org/10.1016/j.micromeso.2008.01.039

[11] Shchemelinina, Tatyana N. – Gömze, László A. – Kotova, Olga B. – Ibrahim, Jamal Eldin F. M. – Shushkov, Dmitry A. – Harja, Maria – Ignatiev, Grigoriy V. – Anchugova, Elena M. (2019): Clay- and zeolite-based biogeosorbents: modelling and properties Építő anyag – Journal of Silicate Based and Composite Materials, Vol. 71, No. 4, pp.131–137. https://doi.org/10.14382/epitoanyag-jsbcm.2019.23

[12] Shushkov, Dmitry A. – Kotova, Olga B. – Ibrahim, Jamal-Eldin F. M. – Harja, Maria – Gömze, László A. – Shchemelinina, Tatyana N. – Ignatiev, Grigoriy V. (2020): Analcime-bearing rocks as advanced sorbents Építőanyag – Journal of Silicate Based and Composite Materials, Vol. 72, No. 5, pp. 156–164. https://doi.org/10.14382/epitoanyag-jsbcm.2020.26

[13] Bouna, L. – Ait El Fakir, A. – Benlhachemi, A. – Draoui, K. – Villain, S. – Guinneton, F. (2020): Physico-chemical characterization of clays from Assa-Zag for valorization in cationic dye methylene blue adsorption, Materials Today: Proceedings, Vol. 22, No. 1, pp. 22–27. https://doi.org/10.1016/j.matpr.2019.08.059

[14] Sakin Omer O., – Hussein M. A., – Hussein B. H. M., – Mgaidi A. (2018): Adsorption thermodynamics of cationic dyes (methylene blue and crystal violet) to a natural clay mineral from aqueous solution between 293.15 and 323.15 K. Arabian Journal of Chemistry, Vol. 11, No. 5, pp. 615–623. https://doi.org/10.1016/j.arabjc.2017.10.007

[15] Fan, H. – Zhou, L. – Jiang, X. – Huang, Q. – Lang, W. (2014): Adsorption of Cu^{2+} and methylene blue on dodecyl sulfobetaine surfactant-modified montmorillonite, Applied Clay Science, Vol. 95, pp. 150–158. doi:10.1016/j.clay.2014.04.001

[16] Hosseinzadeh H., – Khoshnood N. (2015): Removal of cationic dyes by poly(AA-co-AMPS)/montmorillonite nanocomposite hydrogel, Desalination and Water Treatment, Vol. 57, No. 14, pp. 6372–6383. https://doi.org/10.1080/19443994.2015.1008052

[17] Chang, J. – Ma, J. – Ma, Q.– Zhang, D.– Qao, N. – Hu, M. – Ma, H. (2016): Adsorption of methylene blue onto Fe3O4/activated montmorillonite nanocomposite. Applied Clay Science. Vol. 119, No. 1, pp. 132–140, https://doi.org /10.1016/j.clay.2015.06.038.

[18] Hechi, E. – Ben Amor, O. – Srasra, E. – Zargouni, F. (2009): Physico-chemical characterization of acid-activated clay: its industrial application in the clarification of vegetable oils. Surf Surface Engineering and Applied Electrochemistry, Vol. 45, pp. 140–144. https://doi.org/10.3103/S1068375509020112

[19] Bhattacharyya, K. G. – Gupta, S. S. (2011): Removal of Cu(II) by natural and acid-activated clays: An insight of adsorption isotherm, kinetic and thermodynamics, Desalination;Vol.272, Issues (1-3), pp. 66–75. https://doi.org/10.1016/j.desal.2011.01.001

[20] Ugochukwu U. C., – Jones, M. D. – Head, I. M. Manning, D.A.C. Fialips, C. I. (2014): Biodegradation and adsorption of crude oil hydrocarbons supported on"homoionic" montmorillonite clay minerals, Applied Clay Science, Vol. 87, pp. 81–86. https://doi.org/10.1016/j.clay.2013.11.022

[21] Dai; H. – Huang, Y. – Huang H. (2018): Eco-friendly polyvinyl alcohol/carboxymethyl cellulose hydrogels reinforced with graphene oxide and bentonite for enhanced adsorption of methylene blue, Carbohydrate Polymers, Vol. 185. pp. 1–11. doi:10.1016/j.carbpol.2017.12.073

[22] Ghosh, K. – Bar, N. – Biswas, A. B. – Das, S. K. (2019): Removal of methylene blue (aq) using untreated and acid-treated eucalyptus leaves and GA-ANN modelling, The Canadian Journal of Chemical Engineering, Vol. 97, Issues 11, pp. 2883–2898. https://doi.org/10.1002/cjce.23503

[23] Elmorsi, T. M. (2011): Equilibrium isotherms and kinetic studies of removal of methylene blue dye by adsorption onto miswakleaves as a natural adsorbent, Journal of Environmental Protection, Vol. 2, No. 6, 2011, pp. 817–827. doi:10.4236/jep.2011.26093

[24] , A. – Bhat, A. H – Naeem, A. – Isa, M. H. – Danish, M. (2018): High surface area mesoporous activated carbon-alginate beads for efficient removal of methylene blue, International Journal of Biological Macromolecules, Vol. 107, Part B; pp. 1792–1799. https://doi.org/10.1016/j.ijbiomac.2017.10.045.

[25] Alver, E. – Metin, A. Ü – Brouers, F. (2020): Methylene blue adsorption on magnetic alginate/rice husk bio-composite. International Journal of Biological Macromolecules; Vol. 154, pp. 104–113. https://doi.org/10.1016/j.ijbiomac.2020.02.330.

[26] Yang, S. – Zhao, D. – Zhang, H. – Lu, S. – Chen, L. – Yu, X. (2010): Impact of environmental conditions on the sorption behavior of Pb (II) in Nabentonite suspensions, Journal of Hazardous Materials, Vol. 183, Issues (1-3), pp. 632–640. https://doi.org/10.1016/j.jhazmat.2010.07.072

[27] Bilgiç, C. (2005): Investigation of the factors affecting organic cation adsorption on some silicate minerals, Journal of Colloid and Interface Science, Vol. 281, No. 1, pp. 33–38. https://doi.org/10.1016/j.jcis.2004.08.038 Nasrullah

Ref.:
Belhadri, Mazouri – **Benguedach**, Abdelkader – **Sassi**, Mohamed: *Performance assessment of adsorbents based on natural bentonite for removal of cationic dye*
Építőanyag – Journal of Silicate Based and Composite Materials, Vol. 75, No. 2 (2023), 75–79. p.
https://doi.org/10.14382/epitoanyag-jsbcm.2023.11

GUIDELINE FOR AUTHORS

The manuscript must contain the followings: title; author's name, workplace, e-mail address; abstract, keywords; main text; acknowledgement (optional)**; references; figures, photos with notes; tables with notes; short biography** (information on the scientific works of the authors).

The full manuscript should not be more than 6 pages including figures, photos and tables. Settings of the word document are: 3 cm margin up and down, 2,5 cm margin left and right. Paper size: A4. Letter size 10 pt, type: Times New Roman. Lines: simple, justified.

TITLE, AUTHOR

The title of the article should be short and objective.

Under the title the name of the author(s), workplace, e-mail address.

If the text originally was a presentation or poster at a conference, it should be marked.

ABSTRACT, KEYWORDS

The abstract is a short summary of the manuscript, about a half page size. The author should give keywords to the text, which are the most important elements of the article.

MAIN TEXT

Contains: materials and experimental procedure (or something similar), results and discussion (or something similar), conclusions.

REFERENCES

References are marked with numbers, e.g. [6], and a bibliography is made by the reference's order. References should be provided together with the DOI if available.

Examples:

Journals:

[6] Mohamed, K. R. – El-Rashidy, Z. M. – Salama, A. A.: In vitro properties of nano-hydroxyapatite/chitosan biocomposites. *Ceramics International.* 37(8), December 2011, pp. 3265–3271, http://doi.org/10.1016/j.ceramint.2011.05.121

Books:

[6] Mehta, P. K. – Monteiro, P. J. M.: Concrete. Microstructure, properties, and materials. *McGraw-Hill*, 2006, 659 p.

FIGURES, TABLES

All drawings, diagrams and photos are figures. The **text should contain references to all figures and tables**. This shows the place of the figure in the text. Please send all the figures in attached files, and not as a part of the text. **All figures and tables should have a title**.

Authors are asked to submit color figures by submission. Black and white figures are suggested to be avoided, however, acceptable.

The figures should be: tiff, jpg or eps files, 300 dpi at least, photos are 600 dpi at least.

BIOGRAPHY

Max. 500 character size professional biography of the author(s).

CHECKING

The editing board checks the articles and informs the authors about suggested modifications. Since the author is responsible for the content of the article, the author is not liable to accept them.

CONTACT

Please send the manuscript in electronic format to the following e-mail address: femgomze@uni-miskolc.hu and epitoanyag@szte.org.hu or by post: Scientific Society of the Silicate Industry, Budapest, Bécsi út 122–124., H-1034, HUNGARY

We kindly ask the authors to give their e-mail address and phone number on behalf of the quick conciliation.

Építőanyag – *Journal of Silicate Based and Composite Materials*, Quarterly peer-reviewed periodical of the Hungarian Scientific Society of the Silicate Industry, SZTE.
http://epitoanyag.org.hu